THE UNIVERSITY OF SYDNEY

MASTER THESIS

Cancellous Bone Density Evaluation using Ultrasound Backscatter from an Imaging System:Exploring the Possibility for Fetal Bone Density Evaluation

---

Author:

Yang ZHENG

Supervisor:

A/Prof. Alistair MCEWAN

A thesis submitted in fulfillment of the requirements

for the degree of Master of Philosophy

in the

Biomedical Engineering and Technology

Electrical and Information Engineering

August 27, 2017

Declaration:

I, Yang ZHENG, declare that this thesis titled, "Cancellous Bone Density Evaluation using Ultrasound Backscatter from an Imaging System:Exploring the Possibility for Fetal Bone Density Evaluation" and the work presented in it are my own. I confirm that:

- This work was done mainly for a research master degree at the University of Sydney. None of the contents has been submitted for any degree in any University or Institution. Except for the referred part or acknowledged part, the other parts presented are finished by myself.
- The idea of using ultrasound imaging system is from Prof. Ralph Nanan, and the in vitro study that using the second harmonics to evaluate backscatter coefficient is inspired by Dr. Xian Long. I acknowledge them for giving useful advice. Except for the discussion, the implementation of the methodologies and all the programming including theoretical calculation and experimental data processing are finished on my own. The figure of fetal bone development is from Zhunan Wang.
- Most part of this thesis has been published or submitted to journal papers or conference papers. And in the journal papers and conference papers, I did most part of the contribution.The list of publications are as follows:

List of Publications:

Journals:

1.Y.Zheng,X.Long, P.Jones, R.Nanan, A. McEwan"A Quantitative Ultrasound Backscatter Measurement for Fetal Femur Bone Density Evaluation: A Simulation Study based on the Biot's Theory ",submitted to Ultrasound in Medicine and Biology.

Conferences:

1. Y.Zheng, R.Nanan and A.McEwan,"A Simulation Study of Ultrasonic Backscatter Coefficients in Cancellous Bone using Multi-element Ultrasound Probe Models", 38th Annual International Conference of the IEEE Engineering in Medicine and Biology Society (EMBC2016), Orlando, Florida, America, Aug.2016.

2.Y.Zheng, X.Long, C.Jin, R.Nanan and A.McEwan,"Apparent Backscatter of Cancellous Bone from Fundamental and Second Harmonics Using an Ultrasound Imaging System",IEEE International Symposium on Biomedical Imaging (ISBI2017), Melbourne, Australia, Apr. 2017.

Signed: Yang Zheng

Date: 28／08／2017

The University of Sydney

Abstract

Electrical and Information Engineering

Electrical and Information Engineering

Master of Philosophy

Cancellous Bone Density Evaluation using Ultrasound Backscatter from an Imaging System:Exploring the Possibility for Fetal Bone Density Evaluation

by Yang ZHENG

Osteoporosis is a common chronic disease and a well known major source of morbility and mortality among the elderly. Low bone density also occurs in infants and small children during development and can be problematically excessive if the fetus experiences issues during pregnancy such as malnutrition, lack of vitamin D and smoking. Currently the only available methodologies for fetal bone density evaluation are Dual-energy X-ray Absorptiometry (DEXA) or Magnetic Resonance Imaging (MRI). Both are sensitive to movement artifacts. DEXA exposes the subjects to significant radiation so is not suggested during pregnancy. Quantitative MRI is noisy, expensive, slow (8-20 mins) and the effects of high field strengths on the developing fetus is unknown. Therefore, the goal of this study is to find a fast, accurate and non-ionizing method for the evaluation of fetal bone density.

In this study, the quantitative ultrasound backscatter coefficient (BSC) was chosen to evaluate bone density using the B-mode ultrasound system. Compared with the speed of sound and ultrasound attenuation in the traditional ultrasound measurement for bone density, the backscatter method is more accessible to central sites such as the human spine and fetal femur bone. Additionally, it has a rapid path to commercialization with the potential to be added as a new feature in the current commercial ultrasound imaging systems for bone density evaluation.

The contributions of this work are:

1. a simulation study was accomplished that compared backscatter coefficients from a single element transducer, a linear array transducer, and a curved array transducer with the change of trabecular thickness and trabecular spacing. An overall similar Pearson correlation (single: $R = 0.94$, $SD = 10.84dB$, linear: $R = 0.92$, $SD = 6.6dB$, curved: $R = 0.95$, $SD = 6.89dB$) between the BSC and porosity was found from three transducers, but the standard deviation (SD) was smaller from the two array probes. This improved standard deviation may result from the wider spatial range of the array transducers.

2. A simulation model using COMSOL for the fetal bone density evaluation was built based on the Biot's poroelastic theory and the backscatter coefficient. The theoretical

backscatter coefficient from the Biot model was calculated with the best available biomechanical parameters from the human femoral cancellous bone and the geometrical features of the fetal femur. This work also proposed a method for compensating the ultrasound signal attenuation from abdominal tissue, femur tissue, amniotic fluid between the probe and fetal femur. The result showed good correlation of BSC ($R = -0.9970$, $P = 2.0058e^{-}04$, $SD = 10.21\%$) and apparent integrated backscatter (AIB) ($R = -0.9469$, $P = 0.0146$, $SD = 10.62\%$) with the porosity. This suggests in vivo ultrasound bone evaluation could be implemented in the current commercial ultrasound B-mode systems.

3. An in vitro study was conducted that compared the backscatter coefficient (BSC), the apparent integrated backscatter (AIB) and the Spectrum Centroid Shift (SCS) from the fundamental backscatter signal and the second harmonics of the ultrasound imaging system. The result from the second harmonics ($R : BSC = 0.7374$, $AIB = 0.6243$, $SCS = -0.6421$) showed better correlation than the fundamental backscatter ($R : BSC = 0.7055$, $AIB = 0.5393$, $SCS = -0.5858$) with a gold standard bone mineral density obtained from DEXA scans of the same samples. An analysis from the Farran cylindrical model and the second harmonics of a rigid cylinder showed the second harmonics has less noise and showed better performance than the fundamental backscatter approach.

In conclusion, the backscatter coefficient from ultrasound imaging showed good correlation in both the simulation studies and the in vitro study. It has the potential to be a convenient, fast, cheap methodology for adult and fetal bone density evaluation.

Acknowledgements

The completion of this work would not be done without the help and support from my supervisors and friends. Therefore, I would like to show my sincere thankfulness to them below.

Firstly, I would like to thank my supervisor A/Prof. Alistair McEwan. Thanks for his patient guidance and encouragement when I met difficulties during research. He would always support students to try to solve hard questions in the biomedical field, and also would like to give advice in time. And I feel grateful for having the chance to present my work at the 38th Annual International Conference of the IEEE Engineering in Medicine and Biology Society (EMBC 2016) and IEEE International Symposium on Biomedical Imaging (ISBI 2017). I would also like to thank my associate supervisor A/Prof. Craig Jin. His spirit of seeking for truth and thinking clearly on every detail really inspired my research a lot. Thanks to the help from Xian Long and Prof. Ralph Nanan for the general idea of this research.

I would like to thank the University of Sydney Faculty Major Equipment Scheme fund for providing the Verasonics Ultrasound System, which is crucial for doing the in vitro experiment. Thanks to the research facilities and support provided by Sydney Imaging Core Research Facility, the University of Sydney's Preclinical Imaging services, the Bosch Institute. Thanks also to the support and advice from the Charles Perkins Center, the University of Sydney and IIT Madras collaboration and BMET institute.

I would also like to show my gratitude to Emeritus Professor Hans Coster and CMS Innovations Pty Ltd. Australia for giving me a casual job which helped cover the daily expenses in my second year. Thanks to the Norman I Price scholarship provided by the University of Sydney Information and Electrical Engineering Department.

Lastly, I acknowledge the selfless love from my parents Wenchun Zheng and Xiaofu Yang. Without the support from them, I would have no chance to study in Australia and shape my mind in the western culture. Special thanks to my friend Yue Xiao, Yingming

Liang, Jingyang Guo, all the people I met in the EIE lab, and the lovely people I met in the Sydney University Bush Walking Club and Roadrunners Outdoor Club. Thanks to their companion, so that I have the unforgettable experience in various Sydney festivals and the happy moments when exploring the landscape around Sydney. Thanks to Li Liu for providing me a comfortable place to stay in Sydney. I hope all my friends would have a wonderful life in the future.

Contents

Declaration of Authorship **i**

1 Introduction **1**

1.1 Motivation 1

1.2 Current Methodologies of Bone Density Evaluation 2

1.3 Brief Introduction of the Femur Bone Structure 7

1.4 Bone Mineral Deficiency: Signs and Changes in Adult Cancellous Bone and Fetal Femur 9

1.5 The Main Contribution of this Work 10

1.6 Thesis Outline 11

2 A Review of Ultrasound Backscatter Methodologies for Bone Density Evaluation **14**

2.1 Introduction 14

2.2 The Backscatter Coefficient Methods 14

2.3 Apparent Backscatter Methods 19

2.4 Frequency Dependence of Backscatter 22

2.5 Methodologies using Backscatter Images 23

2.6 Other Backscatter Parameters Related to Bone Mineral Density 24

2.7 Comparision of the Methods and Conclusion 25

3 Backscatter Coefficient of Cancellous Bone with the Change of Trabecular Thickness and Spacing: A Comparison Study of Three Probe Models in Simulation **27**

3.1 Introduction 27
3.2 The Geometry of Ultrasound Probes 28
3.3 The Simulation Study using three Probe Models 29
3.4 The Simulation Result and Discussion 32
3.5 Conclusion 33

4 A Quantitative Ultrasound Backscatter Measurement for Fetal Femur Bone Density Evaluation: A Simulation Study based on the Biot's Theory 35
4.1 Introduction 35
4.2 Methodology 38
4.3 Results 46
4.4 Discussion 46
4.5 Conclusion 48

5 A Comparison Study of Ultrasound Backscatter Measurement of Cancellous Bone using the Fundamental Backscatter and the Second Harmonics 50
5.1 Introduction 50
5.2 Background on Second Harmonics 51
5.3 The Fundamental Backscatter and the Second Harmonics from a Cylinder Model 53
5.4 Methodology of the In Vitro Experiment 58
5.5 Results and Discussion 62
5.6 Conclusion 65

6 Conclusion and Future Work 66
6.1 Conclusion 66
6.2 Future Work 67

List of Figures

1.1 The Bone Fracture Sites . . . 3
1.2 The Sketch of Bones at Sites that have High Fracture Risk [1] . . . 3
1.3 The DEXA Image of Adult Proximal Femur [2] . . . 4
1.4 The CT Images on the Clinical, Micro and Nano Scale: (a) is the 3D image of an adult human spine [3], (b) is the microCT Image of the iliac crest bone sample from a menopausal woman [4], (c) is the nanoCT image of a rat distal femur [5] . . . 4
1.5 The MRI Image of a Ovine Hind Limb Bone [6] . . . 5
1.6 The Ultrasound Methodologies of Bone Density Measurement: (a) is the broadband quantitative ultrasound attenuation image of adult calcaneus [7], (b) is the ultrasound measurement using speed of sound on a neonate [8], (c) is the ultrasound measurement using a single probe on a neonate arm based on the speed of sound method [9] . . . 6
1.7 The Development of Fetal Femur [10] . . . 8
1.8 The Structure of Cortical Bone and Cancellous Bone in the Human Femur [11] . . . 8
1.9 The Change of Bone Microstructure due to Bone Mineral Deficiency: the left one is the cancellous bone of lumbar spine from a 23 years old woman while the right one is from a 76 years old female [12]. . . . 9

2.1 Setting for the Ultrasonic Backscatter Coefficient Measurement [13] . . . 15
2.2 The Backscatter Measurement on Human Calcanous [14] . . . 16

3.1 The Properties of the Ultrasound Probes:(1) is the single element probe, (2) is the linear array probe and (3) is the curved array probe.Kerf is the space between two piezo-electric transducer elements 28
3.2 The Linear Array Probe and the Focal Zone 29
3.3 The Cylindrical Bone Model 29
3.4 The Simulation Models of Three Transducers 30
3.5 The Correlation of the Backscatter Coefficient from Three Ultrasound Probe Models with the Porosity of group 3:(1) is the backscatter coefficient from the single element transducer, (2) is the backscatter coefficient from the linear array transducer, (3) is the backscatter coefficient from the curved array transducer. 32

4.1 The Development of Fetal Femur 36
4.2 The Pressue Pulse from the Transducer Elements 40
4.3 Correlation between the Theoretical Reflection Coefficient and the Bone Porosity 42
4.4 B-mode Ultrasound Image of Fetal Femur from a Clinical Study 43
4.5 Simulation Model of Fetal Femur 43
4.6 The Wave from the Transducer Elements 43
4.7 The Backscattered Wave from Femur 43
4.8 The Gated Backscatter Signal 45
4.9 The Power Spectrum of the Backscatter Signal 45
4.10 The Correlation between Backscatter Coefficient and Porosity 45
4.11 The Correlation between Apparent Integrated Backscatter and Porosity . . 45
4.12 The Signal to Noise Ratio 45

5.1 The Distortion of the Sine Wave 51
5.2 The Cylindrical Model that Represent Trabeculae. "a" is the trabecular thickness 53

5.3 The Angular Distribution of Scattering from the Surface of Two Cylinder Models. $f0$ is the central frequency, $f_{2\omega}$ is the 2nd harmonics. The reference pressure is from water $1u\ Pa$ 57
5.4 The Correlation between the Sound Pressure of the Fundamental Backscatter and the 2nd Harmonics with the Change of Cylinder Radius. 57
5.5 The Prepared Bone Samples 58
5.6 The Backscatter Measurement of Cancellous Bone using an Ultrasound Imaging System 59
5.7 The B-mode Ultrasound Images from the Fundamental Backscatter (left) and the Second Harmonics (right). The Selected Region is the Region of Interest. 60
5.8 The Correlation with BMD: (a) BSC from the fundamental backscatter signal. (b) BSC from the second harmonics. (c) AIB from the fundamental signal. (d) AIB from the second harmonics. (e) SCS from the fundamental signal. (f) SCS from the second harmonics. 63

List of Tables

1.1 The Comparison of Four Bone Evaluation Methods 6
1.2 The Variation Range of Trabecular Bone Microstructure 10

2.1 The Correlations Between Bone Mineral Density and Backscatter Parameters 18
2.2 The Correlations between Bone Mineral Density and Integrated Backscatter Parameters 21
2.3 The Frequency Dependence of Ultrasonic Backscatter Coefficient 22
2.4 Correlation between Backscatter Coefficients Images with Bone Mineral Density 24
2.5 Other Backscatter Parameters Related to Bone Density 24

3.1 Multi-element Probe Parameters 31
3.2 The Absolute Correlation Coefficients between Backscatter Coefficients and the Porosity 33

4.1 Biot-Stroll Model Parameters 42
4.2 Geometrical and Acoustical Properties of Fetal Femur Model 44

5.1 Parameters for Theoretical Calculation 56
5.2 Property of the Transducer 61

List of Abbreviations

A/D	**A**nalog to **D**igital
AIB	**A**pparent **I**ntegrated **B**ackscatter
BMD	**B**one **M**ineral **D**ensity
BPD	**B**i**P**arietal **D**iameter
BS/BV	**B**one **S**urface / **B**one **V**olume
BSC	**B**ack**S**catter **C**oefficient
BUA	**B**roadband **U**ltrasound **A**ttenuation
BUB	**B**roadband **U**ltrasonic **B**ackscatter
BV/TV	**B**one **V**olume/**T**issue **V**olume
CAS	**C**ombined **A**pparent integrated backscatter and **S**pestrum centroid shift
CT	**C**omputed **T**omography
DEXA	**D**ual-**E**nergy **X**-ray **A**bsorptiometry
FL	**F**emur **L**ength
FSAB	**F**requency **S**lope of **A**pparent **B**ackscatter
HC	**H**ead **C**ircumference
IBC	**I**ntegrated **B**ackscatter **C**oefficient
MBD	**M**ean of the **B**ackscatter **D**ifference
MRI	**M**agnetic **R**esonance **I**maging
QUS	**Q**uantitative **U**ltra**S**ound
RF	**R**adio **F**requency
SCS	**S**pectral **C**entroid **S**hift
SD	**S**tandard **D**eviation
SOS	**S**peed **O**f **S**ound

Tb.N **T**rabeculae **N**umber

Tb.Sp **T**rabecular **S**pacing

Tb.Th **T**rabecular **T**hickness

TSAB **T**ime **S**lope of **A**pparent **B**ackscatter

UBV **U**ltrasonic **B**one **V**elocity

List of Symbols

a	cylinder diameter	m
A'	aperture area	mm^2
a_{at}	empirical attenuation coefficient of abdominal tissue	Np/cm
a_{aw}	empirical attenuation coefficient of amnionic fluid	Np/cm
a_{ft}	empirical attenuation coefficient of femur tissue	Np/cm
A_{com}	attenuation compensation for tissue	Np/cm
$c0$	speed of sound in water	$1540\,m/s$
$C(f)$	attenuation compensation	Np/cm
d	element center to center distance	mm
F	focal length	cm
$f0$	central frequency	MHz
$Factors(f)$	volume compensation	
G	shear modulus of solid frame	GPa
$I_B(f)$	power spectra of bone	Pa^2
$I_R(f)$	power spectra of reference phantom	Pa^2
Jm	Bessel function	
k	number of wave	
Kb	bulk modulus of solid frame	GPa
Kf	bulk modulus of fluid	GPa
ki	propagation constants of fast and slow wave	
Ks	bulk modulus of grains	GPa
L	gate length	cm
Nm	Neumann function	

P_{biot}	Biot elastic constants P	
P_{in}	pulse amplitude	Pa
$Porosity$	bone porosity	
P_{size}	pore size	m
Q_{biot}	Biot elastic constants Q	
R_{biot}	Biot elastic constants R	
$Rco(w)$	reflection coefficient	
T	amplitude transmission coefficient	
x_{at}	thickness of abdominal tissue	cm
x_{aw}	distance of amnionic fluid	cm
x_{ft}	thickness of femur tissue	cm
V_{com}	volume compensation for array transducer	
w	width of element	mm
z	length of attenuation path	cm
$\alpha_B(f)$	attenuation coefficient of Bone	Np/cm
$\alpha_R(f)$	attenuation coefficient of reference phantom	Np/cm
$\mu_B(f)$	apparent backscatter coefficient	dB/cm
β	coefficient of nonlinearty	
η	angle phase	rad
$\eta_R(f)$	backscatter coefficient of phantom	dB/cm
κ	permeability	cm^2
$\boldsymbol{\mu}$	displacement of the solid material	m
μ_f	fluid viscosity	$Pa \cdot s$
ϕ	angle between the propagation direction and the observation point	rad
ρ_f	density of fluid	kg/m^3
σ	total stress tensor	Pa
τ	tortuosity	
$\boldsymbol{w}$	displacement of the fluid	m

φ	sediment porosity

Chapter 1

Introduction

1.1 Motivation

Osteoporosis is a common chronic disease among the elderly. In Australia in 2012, there were 4.74 million elderly people with osteoporosis, osteopenia or other bone health diseases, and this number represents 66% of the population over 50. In the global point of view, the cost for bone related disease is a massive burden for each country and family. It is estimated that it cost 0.83% of the global burden and 1.75% of the burden in Europe in 2012. Additionally, it is one of the main sources of morbility and mortality in aged groups [15].

Decrease of the bone density occurs not only in elderly people, but in all age groups. Osteoporosis is more common in the elderly group and postmenopausal women [16], however secondary osteoporosis is also found in adolescents and the middle-aged that result from medication, Vitamin D deficiency, gastrointestinal symptoms [17] and diabetes [18]. Low bone density leads to high risk of fracture, the degradation of bones such as the spine [19], and thorax bones that might cause secondary diseases such as hump, thoracic cage deformity and chest compression [20].

Low bone density also occurs in infants and small children due to maternal factors such as malnutrition [21], lack of vitamin D and smoking [22]. The fetal bones are developed from cartilage anlagen, and during the gestational period, it is very sensitive to the maternal environment and extrinsic factors such as the concentration of nutrition, hormone, movement and external stress [23]. The instability of the maternal or external

environment during pregnancy might cause osteomalacia [24].

However, except for MRI, currently there is no other non-ionizing methodology available for the evaluation of fetal bone density. The interference from the maternal bone and tissue, and the fetal movement makes fetal bone evaluation difficult. The fetal bone density could be evaluated using Xrays but these are not suggested for usage during pregnancy [25]. MRI is noisy, expensive, comparatively slow (20-45 minutes) and the long-term effect remains unclear. Moreover, the fetal movement would bring artifacts that would affect the image quality [26]. In the last 20 years, the ultrasound backscatter coefficient (BSC) has shown potential to evaluate bone mineral density. Compared with DEXA and MRI, it is cheap, portable and fast. The feature of using only a single probe makes it accessble to central skeleton sites as well as fetal femur bone. Therefore, in this study, the ultrasound backscatter was chosen as the method to measure bone density.

The ultimate research goal of this study is to find a possible way to evaluate fetal bone density using ultrasound backscatter. In this research, the fetal femur bone, which is widely studied, easy to recognize and representative to the fetal body development, is selected as the region of interest. The B-mode ulrasound system, which is commonly used for fetal examination, was chosen for fetal bone density evaluation. And a method of signal attenuation compensation during ultrasound propagation in maternal and femoral tissue is proposed. Apart from the fetal bone density evaluation, this research also compared the backscatter signal, that is reflected from the fundamental backscatter and the second harmonics, to find the signal that is more accurate for bone density evaluation. The result show that the ultrasound backscatter coefficient has potential to evaluate fetal bone density.

1.2 Current Methodologies of Bone Density Evaluation

The sites (Fig. 1.1) that have high fracture risks are where the current studies and commerical products have focused on for bone mineral desity evaluation. These sites include: proximal femur, lumbar spine, distal radius, mid radius and calcaneus (Fig. 1.2).

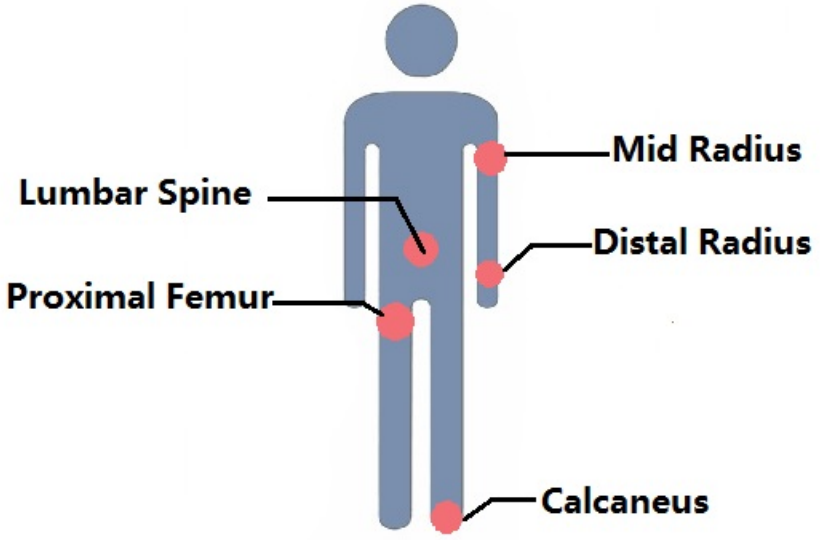

FIGURE 1.1: *The Bone Fracture Sites*

(A) *Spine* (B) *Femur* (C) *Mid Radius* (D) *Distal Radius* (E) *Calcaneus*

FIGURE 1.2: *The Sketch of Bones at Sites that have High Fracture Risk [1]*

The current available methodologies for BMD evaluation are compared below in terms of radioactivity, scanning time, portability and accessibility to central skeleton sites :

Radiological Methods:

∗ **Dual-energy X-ray absorptiometry (DEXA)**

DEXA is regarded as the gold standard and the most common technique for adult bone density evaluation. The DEXA system has mainly two parts to generate a DEXA image: one is the X ray source and another one is the multiple detector array for X-ray collection. The source transmits x-rays with two different energy levels. The attenuation is calculated by the subtraction of the two images different energy levels with a weighted difference [27], then compares the result with a reference database based on gender, race and age (Fig. 1.3). The DEXA-derived measurement is areal bone mineral density (BMD,

FIGURE 1.3: *The DEXA Image of Adult Proximal Femur [2]*

g/cm2).

DEXA scan is quick , not expensive, but the main problem is that it is a radiological method, leading to limited access for pregnant women and vulnerable patients. And it is not portable and can not show bone micro structure very clearly.

∗ **Computed Tomography (CT)**

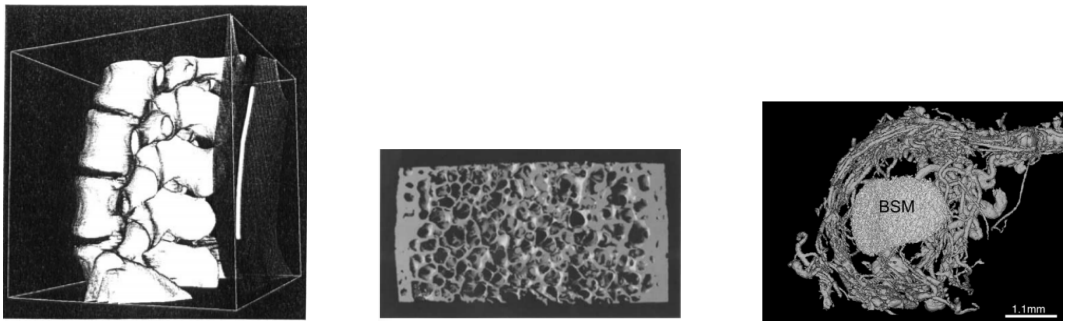

(a) *(b)* *(c)*

FIGURE 1.4: *The CT Images on the Clinical, Micro and Nano Scale: (a) is the 3D image of an adult human spine [3], (b) is the microCT Image of the iliac crest bone sample from a menopausal woman [4], (c) is the nanoCT image of a rat distal femur [5]*

CT is the most accurate way for bone evaluation in terms of bone microstructure. It uses X ray absorption from the different circular angles and reconstruct the structure from the signal in multiple transverse planes. The accuracy of CT has three levels with increasing resolution: the clinical level, the micro level and the nano level. In the clinical level, CT with voxel size ranges from 250-500 μm,is able to reconstruct macro-level bone structure like skull, lumbar and bone cracks. As for the micro level, the HR-pQCT with

voxel size down to 82 μm [28], is able to reconstruct the peripheral bone micro structure such as the trabeculae and the bone frame inside the cortical bone (Fig. 1.4). The CT measurement is volumetric BMD (g/cm3).

Non-Ionizing Methods:

∗ **Magnetic Resonance Imaging (MRI)**

FIGURE 1.5: *The MRI Image of a Ovine Hind Limb Bone [6]*

MRI is a widely applied non-invasive and accurate imaging modality. It is also a tomography imaging system which uses the magnetic field, radio wave and field gradients to generate images [29]. The nuclear-magnetic-resonance-active (NMR-active) atoms such as hydrogen atoms and calcium atoms generate signals which will be encoded by Larmor frequecy and phase difference to reconstruct the tomography images [30]. Hydrogen atoms are the most common in human fat and tissue, the different amount of the generated radio wave in MRI imaging is able to represent the different concentration of the atom which indicates the variance in density.

MRI is comparatively expensive and time-consuming, but it also provides very accurate density and location of the bone (Fig. 1.5). Apart from the MRI system, there are also portable MR systems available for bone density evaluation, such as the MR coil that used on the arms and feet. These systems are also lower cost and fast, however, they are not able to provide longitudinal bone images.

∗ **Quantitative Ultrasound (QUS)**

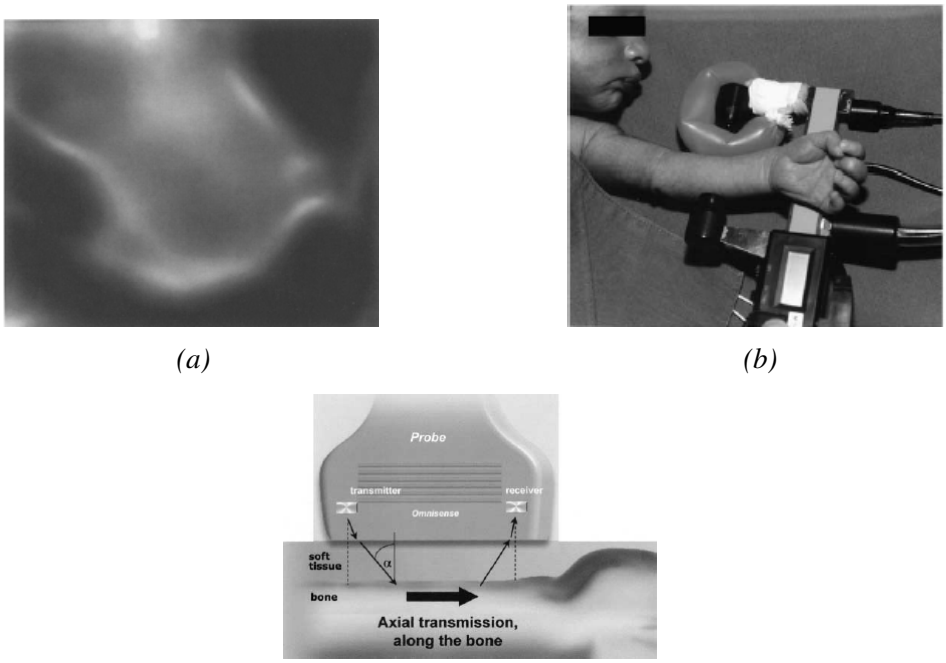

(a) *(b)* *(c)*

FIGURE 1.6: *The Ultrasound Methodologies of Bone Density Measurement: (a) is the broadband quantitative ultrasound attenuation image of adult calcaneus [7], (b) is the ultrasound measurement using speed of sound on a neonate [8], (c) is the ultrasound measurement using a single probe on a neonate arm based on the speed of sound method [9]*

TABLE 1.1: *The Comparison of Four Bone Evaluation Methods*

Properties	**MRI**		**CT**		**Ultrasound**		**DEXA**
	Imaging	**Coil**	**CT**	**HR-pQCT**	**BUA, SOS**	**Backscatter**	
Ionizing	No	No	Yes	Yes	No	No	Yes
Expense	Highest	Low	High	High	Low	Low	Medium
Time	8-20 mins	15 mins	2-10 mins	2.8mins [28]	$<$ 5 mins	$<$ 5 mins	3-5 mins
Portability	No	Yes	No	No	Yes	Yes	No
Micro Structure	No	No	Yes	Yes	No	No	No
Providing Bone Location	Yes	Yes	Yes	Yes	Yes in Image	No	Yes
Accessible to central sites	Yes	No	Yes	Yes	No	Yes	Yes

The current bone density methodologies using ultrasound are mainly based on the two features: the speed of sound (SOS) in bone and the broadband ultrasound attenuation (BUA). Ultrasound is inexpensive among the four imaging technologies and the portability is also the reason for its wide application.

The transmit and receive method is applied in quantitative ultrasound. When the transmitted wave passes through the bone, the bone microstructure and bone soft tissue distort and damp the wave, resulting in the change of pulse speed and attenuation. The current devices available include a quantitative imaging system which has multiple ultrasound elements that is used for calcaneus cancellous bone evaluation. It provides images based on the local absorption and attenuation of ultrasound signal, but it is not accurate enough to determine the microstructure. There are other systems available that clamp on the arm to measure the speed of sound or combine the transmit and receive transducer in a single probe (Fig. 1.6).

Apart from the methodologies using SOS and BUA, the ultrasound backscatter has raised research interest because it is more flexible for the evaluation of central skeleton sites. This method evaluates the bone density using the backscattered signal based on ultrasound attenuation, backscatter coefficient and spectral centroid shift. This is widely applied in the quantitative ultrasound of the soft tissue and this methodology has already achieved various degrees of success.

The features of the four methodologies introduced above are summarized in Table 1.1. Compared with DEXA, MRI, CT, the ultrasound backscatter is non-inoizing, portable, cheap, fast and accessible to the central skeleton sites as well as the fetal bone. Therefore, in this study, the ultrasound backscatter is selected as the methodology for fetal bone density evaluation.

1.3 Brief Introduction of the Femur Bone Structure

The fetal femur bone development starts with the appearance of limb buds, after 6-9 weeks, it develops to the cartilage anlagen which is the embryonic form of femur bone (Fig. 1.7). Then the bone collar starts to form at the central shaft which becomes the center of the first stage ossification [31]. The collar prevented the absorption of nutrition in the center which leads to the cavity, and the cavity is then occupied by the blood vessels. So the ossification area begins to expand towards the ends of the long bone. In

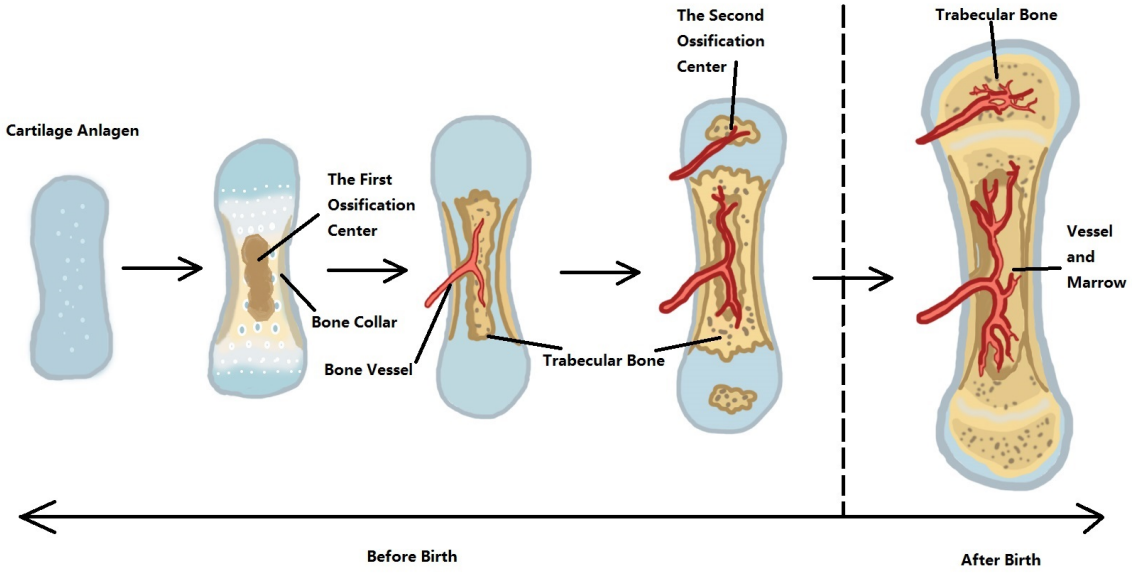

FIGURE 1.7: *The Development of Fetal Femur [10]*

the last stage of prenatal femur bone development, the center of the secondary ossification forms at the end of the bone. The secondary ossification starts from 2-4 months after birth, and then the ossification starts to show at the proximal epiphysis and the greater trochanter [23].

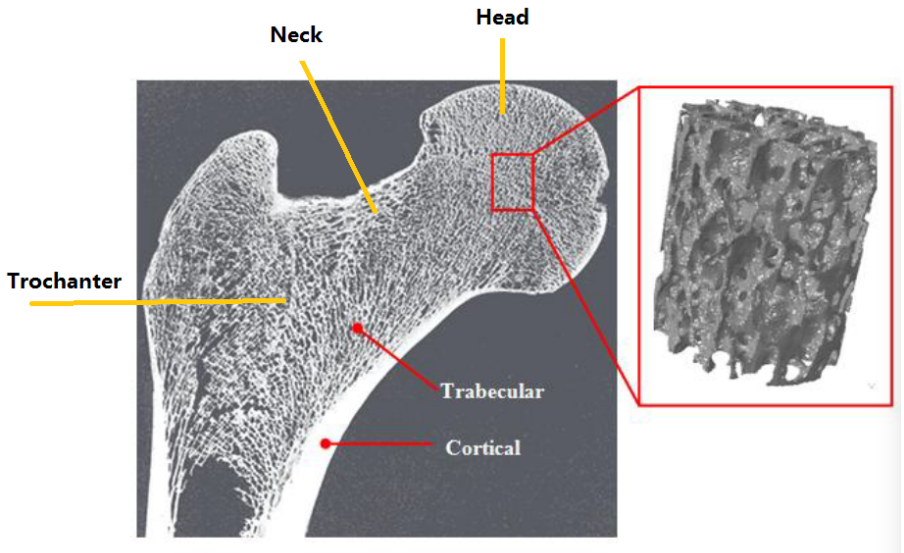

FIGURE 1.8: *The Structure of Cortical Bone and Cancellous Bone in the Human Femur [11]*

The adult femur bone is shown in Fig. 1.8. The spongy part of the bone is at the

femur neck, trochanter and head. The ultrasound with the frequency below 5MHZ is able to penetrate through because of the comparatively low attenuation caused by the cortical layer. The spongy bone inside is also called trabecular bone because of its structure. The trabecular bone is composed of multiple inter-connected small beams or rods. The beams are called the trabeculae while the space between the trabeculae is the trabecular spacing (Tr.Sp).

1.4 Bone Mineral Deficiency: Signs and Changes in Adult Cancellous Bone and Fetal Femur

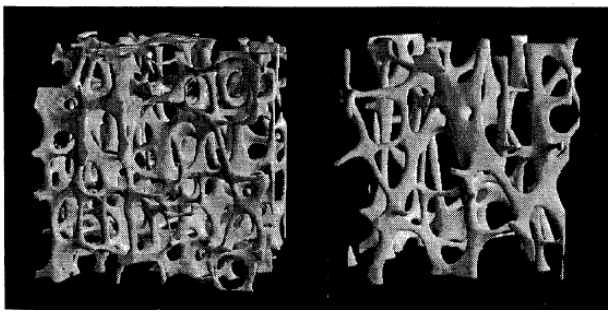

FIGURE 1.9: *The Change of Bone Microstructure due to Bone Mineral Deficiency: the left one is the cancellous bone of lumbar spine from a 23 years old woman while the right one is from a 76 years old female [12].*

The microstructure of the human cancellous bone (Fig. 1.9) is described by the following features:

•Trabecular Thickness (Tb.Th): The average thickness of the rod structure which composed the bone frame.

•Trabecular Spacing (Tb.Sp): The average space between the two trabeculae.

•Trabeculae Number (Tb.N): The number of trabeculae.

•Bone Volume/Tissue Volume (BV/TV): The ratio of the bone tissue volume over the whole tissue volume including fat and marrow.

•Connectivity: The ratio of interconnected trabecular structure.

TABLE 1.2: *The Variation Range of Trabecular Bone Microstructure*

Adult Trabecular Femur Bone		**Fetal Intact Femur**	
Parameter	**Variation Range**	**Parameter**	**Variation Range**
Tb.Th	90-265 *um* [32]	Tb.Th	84.2-118.2**um* [33]
Tb.Sp	38-123 *um* [32]	Tb.Sp	155.2-321.2**um* [33]
Tb.N	0.78-1.68 [32]	Tr.N	$--$
BV/TV	8.5-42 % [32]	BV/TV	29.8-54*% [33]
BMD	22-206 mg/cm^2 [34]	BMD	15-230*mg/cm^2 [35]

[1] The adult trabecular bone properties is obtained from human proximal femur with the age ranges from 40-90 years old.
[2] The fetal bone properties marked with $*$ is measured in the second trimester, while the properties marked with $\star$ is obtained in the second and the third trimester including the cortical bone.

The parameters available from previous studies of the change of human bone microstructure of the femur is summarized in the Table 1.2. In summary, with the increase of bone porosity, the changes in the bone microstructure are the decrease of the trabecular thickness, trabeculae number, BV/TV and the connectivity and the increase of the trabecular spacing.

1.5 The Main Contribution of this Work

1. A simulation study was accomplished that compared backscatter coefficients from a single element transducer, a linear array transducer, and a curved array transducer. This model evaluated the correlation of BSC from three probes against a range of porosities defined by trabecular thickness and trabecular spacing. The Pearson correlation (R) and standard deviation (SD) from three transducers were: single element ($R = 0.94$, $SD = 10.84dB$), linear array ($R = 0.92$, $SD = 6.6dB$) and curved array ($R = 0.95$, $SD = 6.89dB$). A similar correlation between the BSC and porosity was found from three transducers, but the standard deviation was smaller from the two array probes. This improved standard deviation may have resulted from the wider spatial range of the array transducers.

2. A simulation model was built using COMSOL for the fetal bone density evaluation using Biot's poroelastic theory and the backscatter coefficient. The theoretical backscatter coefficient from the Biot model was calculated with the best available biomechanical parameters from the human femoral cancellous bone and the geometrical features of the fetal femur. This work also proposed a method for compensating the ultrasound signal attenuation from abdominal tissue, femur tissue, amniotic fluid between the probe and fetal femur. The result showed good correlation of BSC ($R = -0.9970$; $P = 2.0058e^{-}04$; $SD = 10.21\%$) and apparent integrated backscatter (AIB) ($R = -0.9469$, $P = 0.0146$, $SD = 10.62\%$) with the porosity. This suggests in vivo ultrasound bone evaluation could be implemented in the current commercial ultrasound B-mode systems.

3. An in vitro study was conducted that compared the backscatter coefficient (BSC), the apparent integrated backscatter (AIB) and the Spectrum Centroid Shift (SCS) from the fundamental backscatter signal and the second harmonics of the ultrasound imaging system. The result from the second harmonics ($R : BSC = 0.7374$, $AIB = 0.6243$, $SCS = -0.6421$) showed better correlation than the fundamental backscatter ($R : BSC = 0.7055$, $AIB = 0.5393$, $SCS = -0.5858$) with a gold standard bone mineral density obtained from DEXA scans of the same samples. An analysis from the Farran cylindrical model and the second harmonics of a rigid cylinder showed the second harmonics has less noise and showed better performance than fundamental backscatter approach.

In conclusion, the backscatter coefficient from ultrasound imaging system showed good correlation in both the simulation studies and the in vitro study. It has the potential to be a convenient, fast, cheap methodology for adult and fetal bone density evaluation.

1.6 Thesis Outline

The outline of the thesis is summarized as follows:

The first chapter is the introduction of the research topic. It briefly summarized currently available methodologies for bone density evaluation and compared them in terms of radioactivity, portability, and accessibility to central sites. It presented the development

process of fetal femur and the change of adult bone micro structure due to bone mineral deficiency. It also introduced the difference between the transmit-through quantitive ultrasound and the ultrasound backscatter, and the reason for chosing ultrasound backscatter as the methodology.

The second chapter reviews algorithms that use the ultrasound backscatter coefficient to obtain the backscatter parameters such as BSC, AIB and SCS. The correlation between the backscatter parameters with the bone density are summarized in Table 2.1-2.5.

The third chapter describes a simulation study to evaluate the backscatter coefficient from three types of transducers: the single element transducer, the linear array transducer, and the curved array transducer. A bone model with changes of trabecular thickness and trabecular space was built and 10 groups of data from each transducer was collected. The result shows that the correlation between the backscatter coefficient and the bone porosity from the three transducers are close to each other. However, due to the wider spectral range of the array transducers, the result from array transducers showed smaller standard deviation.

The fourth chapter introduces a simulation model that may be applied for fetal bone density evaluation using array ultrasound transducer. This fetal bone model was based on the Biot poroelastic theory, and it was built based on the real size and biomechanical properties of human femoral cancellous bone. A signal intensity compensation methodology for the attenuation during the propagation in the abdominal tissue, fetal femoral tissue and amniotic fluid is proposed. The simulation result was compared with the theoretical result of reflection coefficient from the Biot model, and it showed good correlation with the change of bone porosity.

The fifth chapter reports an in vitro experiment that compared the backscatter coefficient from the bovine cancellous bone specimens using the fundamental backscatter and the second harmonics. The second harmonics is widely utilized in the B-mode ultrasound imaging, and it has less noise than the fundamental signal. In this study, the BSC, AIB and SCS from the second harmonics showed better correlation than the signal from the fundamental backscatter.

The sixth chapter is a conclusion of this work and it also lists possible future work of this research.

Chapter 2

A Review of Ultrasound Backscatter Methodologies for Bone Density Evaluation

2.1 Introduction

The ultrasound backscatter coefficient (BSC) was previously studied to characterize tissue properties such as tissue density to classify disease. In the last 20 years, this methodology was applied to the cancellous bone and achieved various levels of success in the correlation with the bone density and bone microstructure. In the early research, a transmit-through method was proposed with the attenuation compensation from the wave that transmitted through the bone. Then a methodology that uses the backscattered wave for attenuation compensation was proposed, followed by the methods that do not need attenuation compensation such as apparent integrated backscatter (AIB) and spectral centroid shift (SCS). The detailed review is given below:

2.2 The Backscatter Coefficient Methods

Detecting bone mineral density using ultrasonic backscatter was first proposed by Roberjot et al. [36] and the testing environment as in Fig. 2.1. In their experiment, the focused broadband ultrasound transducer pair was used to capture signal transmitted

through and scattered back from human calcaneus specimens with the frequency range of $200-600kHZ$. The Integrated Backscatter Coefficient (IBC) was calculated as the averaged backscatter coefficient with attenuation compensation using the signal transmitted through the bone. A moderate correlation ($R^2 = 0.68$) was found with BMD.

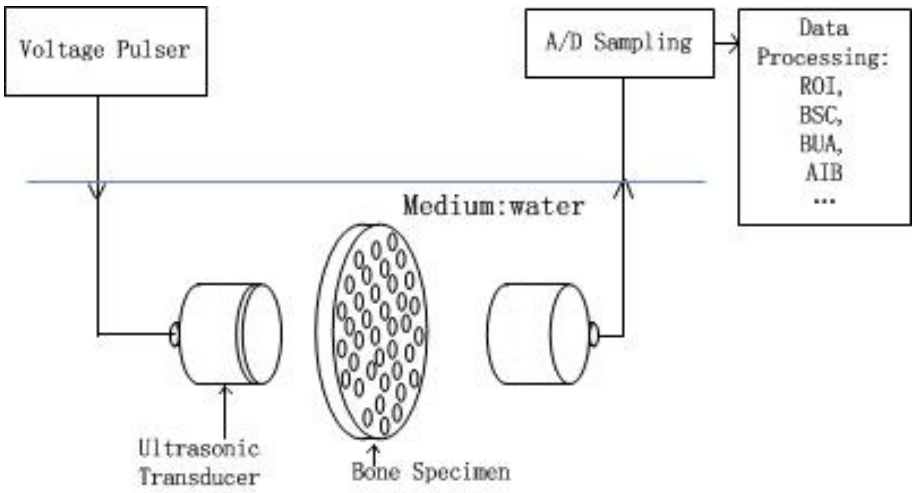

FIGURE 2.1: *Setting for the Ultrasonic Backscatter Coefficient Measurement [13]*

In 1998, Wear et al. [37] proposed a reference backscatter coefficient method (BSC) which used a phantom with known attenuation efficient and frequency-dependent backscatter coefficient as the reference. Unlike Roberjot's work which used transmitted through signal as attenuation compensation, Wear's work only used backscatter signals. The calculation of backscatter coefficient [38] is as follows:

$$BSC(f) = \frac{1}{T^4}\frac{G[\alpha(f),L]}{G[\alpha_{ref}(f),L]}\frac{S_B(f)}{S_{ref}(f)}BSC_{ref}(f) \tag{2.1}$$

Where $G[\alpha(f),L]$ is the function for attenuation compensation, T is the amplitude transmission coefficient of the interface of water and bone. $BSC_{ref}(f)$ is the known backscatter coefficient in the reference phantom. $S_B(f)$ and $S_{ref}(f)$ are the power spectra of backscatter from bone specimens and reference phantom, respectively.

$$G[\alpha(f), l] = \frac{4\alpha(f)L}{1 - e^{-4\alpha(f)L}} \tag{2.2}$$

In the attenuation compensation function (Eq. 2.2), $\alpha(f)$ stands for attenuation coefficient, L stands for gated length of RF data.

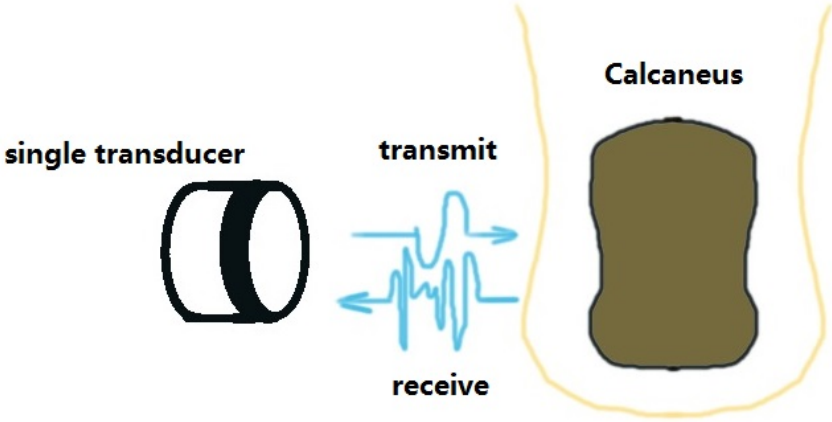

FIGURE 2.2: *The Backscatter Measurement on Human Calcanous [14]*

Then Wear et al. conducted a series of reference backscatter experiments both in vivo [39] and in vitro [40–42]. Broadband ultrasonic transducer pair was used for all the following experiments. The aim of these experiments were to find the correlation of BSC with the ultrasonic attenuation (BUA), the speed of sound (SOS) and the bone microstructure. These experiments confirmed that BSC is in moderate to strong correlations ($R = 0.5 - 0.87$) with BMD, and it may also provide information about trabecular thickness [42].

Chaffai [14, 43] (Fig. 2.2) proposed a method that uses the reference signal from a perfect reflector for ultrasonic backscatter coefficient calculation:

$$BSC(f) = \hat{\mu}_B(f)C(f)Factors(f) \tag{2.3}$$

Where $\hat{\mu}_B(f)$ stands for the apparent backscatter coefficient, $C(f)$ stands for the attenuation compensation and Factors(f) stands for the frequency-dependent scattering volume correction.

The apparent backscatter coefficient is calculated as follows, it is a logarithm ratio of gated power spectra from bone samples and a perfect reflector.

$$\hat{\mu}_B(f) = 8.68ln\frac{S_B(f)}{S_{ref}(f)} \tag{2.4}$$

$$C(f) = e^{4\alpha(f)(z)}\frac{4\alpha(f)L}{e^{2\alpha(f)L} - e^{-2\alpha(f)L}} \tag{2.5}$$

$$Factors(f) = \frac{1}{(0.63)^2}\frac{k^2 r_t^2}{8\pi d[1+(\frac{ka^2}{4F})^2]} \tag{2.6}$$

For the attenuation compensation function and the scattering volume correction function, $\alpha(f)$ is the attenuation coefficient of bone, L is the gate length. r_t is the transducer radius, wave number $k = 2\pi/\lambda$, z is the attenuation path from bone surface to the gated volume, F is the focal length, $(1/0.63)^2$ stands for the compensation for hamming window.

Broadband ultrasonic backscatter (BUB) is the averaged backscatter coefficient in the frequency range of the transducer. BUB is defined as function (Eq. 2.7), in which f_{max} and f_{min} stand for the maximum value and the minimum value of transducer bandwidth, respectively.

$$BUB = \frac{\int_{f_{min}}^{f_{max}} BSC(f)df}{f_{max} - f_{min}} \tag{2.7}$$

TABLE 2.1: *The Correlations Between Bone Mineral Density and Backscatter Parameters*

Author. Year .Ref	Frequency (HZ)	Transducer	The Correlation Coefficient with BMD (R)				
			BSC	nBUA	UBV	BUB	Other Parameters
Roberjot et al. 1996. [36]	200-600K	single	––	0.74*	0.88*	––	IBC:0.68*
Wear et al. 1998. [37]	2.25M	array	0.87	––	––	––	––
Wear et al. 1999. [40]	500K	single	0.81	0.81	––	––	––
Wear et al. 2000. [41]	500K	single	––	0.84	0.84	––	––
Wear et al. 2001. [39]	1M	single	0.5	0.56	0.51	––	––
Roux et al. 2001. [44]	––	single	––	0.54	0.32	0.34	––
Chaffa et al. 2002. [14]	500K	single	––	0.84*	0.9*	0.89*	––
Jenson et al. 2004. [45]	1M	single	––	0.79*	0.74*	0.61*	––
Hakulinen et al. 2005. [13]	0.2–6.7 M	single	––	0.56-0.70	0.51-0.82	0.54-0.81	IRC: 0.70-0.85
Padilla et al. 2008. [46]	1M	single	––	0.79	0.74	0.61	––
Conversano et al. 2015. [47]	3.5M	array	––	––	––	––	O.S.score: 0.866
Zhang et al. 2013. [48]	5M	array	BSC with gestational age (R=0.47), birth weight (R=0.47,) and length at birth (R=0.43)				

BSC stands for the backscatter coefficient, nBUA stands for the slope of frequency-dependent attenuation coefficient, UBV stands for the ultrasonic bone velocity, BUB stands for the broadband ultrasound backscatter, IBC stands for the integrated backscatter coefficient, IRC stands for the integrated reflection coefficient. The square of the correlation coefficient R^2 is marked with "$*$"

Compared with Wear's method, the measurement of attenuation in Chaffai's method do not need reference from a phantom, which makes the calculation of BSC using the signal from a single transducer more flexible. This approach was adopted by [13,45,46,48]. All the following experiments showed good correlations between BSC and BMD. Roux et al. [44] found that the BSC from calcaneus is in moderate to low correlation (R=0.34)

of BMD in lumbar spine and hip of postmenopausal women. They claimed that the low correlation is resulted from the variability of backscatter source. Zhang et al. [48] found that BSC correlates with birth weight (R=0.47) as well as length at birth (R=0.43) of neonates, which implies that BSC is feasible to detect bone status in neonates. Conversano et al. [47] achieved good result (R=0.866) using a novel osteoporosis score (O.S), they compared the backscatter spectrum from the osteoporotic group with the spectrum from the healthy control group to determine the degree of osteoporosis. The result is summarized as in Table 2.1.

From Table 2.1 we could see 9 out of 12 experiments used single transducer and most of them used comparatively low frequency (below or equal to 1MHZ) which is not within the frequency range for the clinical ultrasound imaging system ($1-18$MHZ). The experiments in vivo (R=0.34-0.866) have lower correlation coefficient when compared with the experiments in vitro (R=0.61-0.87).

2.3 Apparent Backscatter Methods

For BSC methods and related backscatter methods, compensation for the attenuation is still necessary for the calculation of BSC. Therefore, a series of experiments using backscatter signals from a single transducer were done for simplified ways of osteoporosis evaluation without compensation. Apparent Integrated Backscatter (AIB) and Spectral Centroid Shift (SCS) which do not need attenuation compensation are alternatives for BSC and BUB.

In the ultrasonic measurement of osteoporosis, QUS uses the ultrasonic backscatter attenuation (BUA) and the ultrasonic bone velocity (UBV) for porosity assessment. SCS is closely related to BUA and UBV and it is a feature of attenuation evaluation in soft tissue. Therefore, Wear [49] adopted this method for bone density characterization. The centroid $\bar{f}$ is written as [50]:

$$\bar{f} = \frac{\int_{f_{min}}^{f_{max}} f * S_B(f) df}{\int_{f_{min}}^{f_{max}} S_B(f) df} \tag{2.8}$$

Where $S_B(f)$ stands for the averaged power spectrum of bone, f_{min} and f_{max} stand for the minimum value and the maximum value of the transducer bandwidth, respectively. The centroid shift is the difference of frequency averaged spectral centroid between the backscatter signals from bone and a perfect reflector:

$$SCS = f_{ref} - \bar{f} \tag{2.9}$$

The effect of SCS was proved by Garra et al. [51], they measured SCS from the spine of 9 women, and the correlation between SCS and BMD is moderate $(R = -0.61)$. Jiang et al. [52] measured SCS on calcaneus of 1011 participants and they got a better correlation (R=-0.70− -0.75). They further proved that BMD correlates better with SCS than with AIB (R=0.55-0.65).

The AIB method was first proposed by Hoffmeister et al. [53]. Similar to SCS, it is a feature that has been extensively studied for tissue characterization. Also, it performs well in the frequency range (2.5-7.5MHZ) which is used for clinical ultrasound image systems. The calculation for AIB is:

$$AIB = \frac{1}{\Delta f} \int_{f_{min}}^{f_{max}} 10 log_{10} \frac{S_B(f)}{S_{ref}(f)} df \tag{2.10}$$

Where f_{max} and f_{min} stand for the maximum and minimum frequencies of transducer bandwidth, $\Delta f = f_{max} - f_{min}$, $S_B(f)$ and $S_{ref}(f)$ stand for power spectrum of backscatter from bone and reference .

Then, a number of in vitro experiments of AIB about frequency dependence [54], and AIB related parameters such as the frequency slope of apparent backscatter (FSAB), and

TABLE 2.2: *The Correlations between Bone Mineral Density and Integrated Backscatter Parameters*

Author. Year.Ref	Frequency (HZ)	Correlation Coefficient with BMD (R)		
		AIB	SCS	other parameters
Wear et al. 2003. [49]	500K	−−	-0.71	−−
Hoffmeister et al. 2006. [53]	1M,5M	5M: transverse:0.817* longitudinal:0.488*	−−	−−
Hoffmeister et al. 2008. [54]	0.6-15.0M	5 M:0.70-0.89 7.5 M: 0 75-0.93	−−	FSAB:2.25 M:(0.70-0.88) 5 M:(0.79-0.94),7.5 M:(0.80-0.92) TSAB:5 M:(0.68-0.89) 7.5 M:(0.75-0.89),10 M:(0.75-0.92)
Garra et al. 2009. [51]	2.5 M	−−	-0.61	−−
Malo et al. 2014. [55]	5M	0.44*	−−	MBD: 0.38 − 0.45*
Jiang et al. 2014. [52]	3.5,5.0M	0.55-0.65	-0.7−-0.75	−−
Tang et al. 2016. [50]	3.5,5.0M	0.51-0.58	-0.66−-0.69	CAS:0.73-0.84

AIB stands for the apparent integrated backscatter, SCS stands for spectral centroid shift, FSAB stands for the frequency slope of apparent backscatter, TSAB stands for the time slope of apparent backscatter, MBD stands for the mean of the backscatter difference, CAS stands for combined AIB and SCS.The square of the correlation coefficient R^2 is marked with "$*$"

the time slope of apparent backscatter (TSAB) [54, 55] and the mean of the backscatter difference (MBD) [55] were studied. Jiang et al. [52] tested both AIB and SCS in vivo on calcaneus, and in this experiment AIB (R=0.55-0.65) is less correlated with BMD than SCS (R=-0.7−-0.75). Tang et al. [50] proposed a new parameter(CAS) that combined AIB and SCS, which is the difference value of weighted AIB and SCS. They claimed that CAS (R=0.73-0.84) is more significant correlated with BMD than AIB (R=0.51-0.58) or SCS (R=-0.66−-0.69).The performance of experiments of AIB and SCS is summarized as Table 2.2.

TABLE 2.3: *The Frequency Dependence of Ultrasonic Backscatter Coefficient*

Author. Year .Ref	Frequency (HZ)	Correlation Coefficient with BMD (R)	
		Theoretical BSC	Other Parameters
Wear et al. 1999. [38]	0.5−2.25 M	−−	−−
Chaffai et al. 2000. [43]	0.4−1.2 M	$0.67-0.99^{*}$	−−
Rederic et al. 2003. [56]	0.4−1.2 M	−−	Tb.Th:$0.51-0.6^{*}$
Lee et al. 2012. [57]	1.4−3 M	−−	−−
Ta et al. 2008. [58]	0.2−5.5 M	0.85	−−
Wear et al. 2008. [59]	0.3−0.7 M	−−	−−
Lee et al. 2013. [60]	0.2−0.7 M	−−	BV/TV :0.76 Tb.Th: 0.77
Sockalin et al. 2010. [61]	5−10 M	−−	−−
Hoffmeister et al. 2011. [62]	1−10 M	−−	AIB and FSAB: 0.570−0.933

Tb.Th stands for trabecular thickness, BV/TV stands for bone volume fraction. The square of the correlation coefficient R^2 is marked with "$*$"

2.4 Frequency Dependence of Backscatter

The typical frequency range for clinical ultrasound imaging systems is 1-18M HZ, However, in the early backscatter studies, the frequency used was low (0.5-1MHZ). Therefore, to make the backscatter coefficient a feature for clinical usage, it is essential to understand the ultrasonic backscatter tendency within the clinical frequency range (Table 2.3).

Wear et al. [38] built a Faran cylindrical model and they proposed that backscatter increases proportionally at lower frequencies (<1MHZ), the increase slows down when it reaches higher frequencies (>5MHz). The frequency dependence of autocorrelation model proposed by Chaffai et al. [43] and statistical weak scattering model proposed by

Rederic et al. [56] reinforced Wear's finding. Lee [57] proposed a binary mixture model and simulated the model using higher frequency range (1.4-3MHZ). The result from their research showed that backscatter coefficient increases within the frequency and decreases with porosity.

Apart from predictions using models, several in vitro and in vivo experiments were conducted. Ta et al. [58] tested the backscatter coefficient both on bovine tibiae and on human calcanei (in vivo, R=0.85). Wear et al. [59] tested BSC using quasi-parallel-nylon-wire phantom. Lee et al. [60] used bovine trabecular bone for experiment (R=0.76-0.77). The trend of these experiments all agrees with the result that first proposed by Wear et al. Sockalin et al. [61] demonstrated that BSC varies significantly with different directions, and BSC does not increase significantly with frequency when over 5MHZ. Frequency dependence of integrated backscatter was studied by hoffmeister [62], the result showed that AIB and FSAB (R=0.57-0.933) are proportional to BMD.

2.5 Methodologies using Backscatter Images

The research interest of backscatter images (Table 2.4) has then increased because compared with BSC from a few different sites, the BSC image is more representative to the BSC of the trabecular bone region and reveals more information of bone density variance. Therefore, Jenson et al. [34] reconstructed images for both QUS parameters (nBUA, SOS) and the backscatter parameter (BSC). Compared with QUS parameters ($R^2 = 0.73 - 0.77$), BSC showed lower correlation ($R^2 = 0.58 - 0.63$) with BMD. Yang et al. [63] built BSC and AIB images of 22 bovine cancellous bones. A Mediate correlation (R=0.556) was found between trabecular spacing and parametric ultrasonic images. Ta et al. [64] correlated BSC in SCS images and they demonstrated that SCS is in mediate correlation (R=0.477-0.699) with all QCT parameters. AIB images were built by Karjalainen et al. [65], it was found significantly correlated ($R^2 = 0.58$) with the bone volume fraction and the collagen content of bone matrix.

TABLE 2.4: *Correlation between Backscatter Coefficients Images with Bone Mineral Density*

Author. Year .Ref	Frequency (HZ)	Correlation Coefficient with BUB (R)	
		BMD	Other Parameters
Jenson et al. 2006. [34]	1−5M	0.58−0.63*	−−
Yang et al. 2009. [63]	10M	−−	Tb.Sp(AIB)-0.556
Ta et al. 2009. [64]	10M	−−	Tb.Th: -0.699 Tb.Sp: 0.477 BV/TV: -0.675 BS/BV : 0.663
karjalainen et al. 2009. [65]	1M	0.58*	−−

BV/TV stands for bone volume fraction, Tr.Sp stands for trabecular spacing , Tb.Th stands for trabecular thickness, BS/BV stands for the ratio of the bone surface in the bone volume. The square of the correlation coefficient R^2 is marked with "$*$".

2.6 Other Backscatter Parameters Related to Bone Mineral Density

TABLE 2.5: *Other Backscatter Parameters Related to Bone Density*

Author. Year .Ref	Frequency (HZ)	Correlation Coefficient with BMD (R)
Riekkinen et al. 2008. [66]	2.25,5.0 M	−−
Hoffmeister et al. 2012. [67]	2.25,5,7.5,10 M	Averaged BSC Apectrum : 0.70−0.95

Riekkinen [66] proposed a dual frequency ultrasound method. Both 2.25M HZ and 5MHZ signals are used for the experiment. They claimed that the dual frequency method is not only able to detect BMD, but also able to determine the thickness of soft tissue, which may enhance the accuracy of BMD using backscatter. Hoffmeister et al. [67] proposed a backscatter difference technique. Two consecutively gated area from the same RF

data were used for calculation. The result showed good correlation (R=0.70-0.95) with BMD (Table 2.5).

2.7 Comparision of the Methods and Conclusion

The common backscatter parameters used in the current available studies are: Ultrasound backscatter coefficient (BSC), apparent integrated baskscatter (AIB), spectrum centroid shift (SCS). And these methodologies are applied for quantitative ultrasound backscatter image evaluation such as the AIB images and the BSC images. In general, the BSC (R=0.5-0.87), AIB (R=0.51-0.817), SCS (R=-0.61−-0.75) correlates well with bone mineral density as well as the bone microstructures such as BV/TV (R=0.63-0.84), Tb.Sp (R=-0.57–0.77), Tb.Th (R=-0.699). The correlation of BSC and SCS are generally better than AIB.

Most of the current studies are using the single element transducer, including the studies for the ultrasound backscatter imaging. And the frequency used in most of the studies are low (<1MHz), which is lower than the frequency that used in the ultrasound imaging system (1-18MHz). The reason for chosing lower frequency is because of the high ultrasound attenuation in bone. The attenuation is larger in the higher frequency, and the BSC does not vary significantly when the frequency is higher than 5MHz. For AIB and SCS, the frequency used are higher (typically 2-5MHz), this is because AIB and SCS are based on apparent backscatter without attenuation compensation, where the backscatter signal is comparetively larger than in lower frequency(<1MHz). For the assessment using backscatter images, the methodologies to obtain BSC, AIB and SCS are using the single element transducer to scan vertically and horizontally at each pixel of the image, which is time consuming.

Apart from the groups using the single element transducer, Zhang et al. [48] and Conversano et al. [47] used the ultrasound imaging system. The ultrasound imaging system are widely applied in the assessment of the BSC from the soft tissue, and the result from the two groups shows that the BSC from the imaging system also correlate well with

the BMD (R=0.866 for O.S score, 0.43-0.47 for fetal weight and length). Therefore, the ultrasound imaging system may be more convenient to evaluate bone density using the ultrasound backscatter.

In conclusion, the ultrasound backscatter is able to provide bone mineral density information. The ultrasound imaging system could be used to obtain backscatter parameters for BMD evaluation.

Chapter 3

Backscatter Coefficient of Cancellous Bone with the Change of Trabecular Thickness and Spacing: A Comparison Study of Three Probe Models in Simulation

3.1 Introduction

The change of the trabecular thickness and the trabecular spacing are two main features of the decrease in the cancellous bone density as well as the bone microstructure. In the studies summarized in the Chapter 2, most QUS bone systems (calcaneus/phalanx) incorporate single-element ultrasound transducers. Current studies are focusing on the peripheral cancellous bones that is easy to access, such as the calcaneus. Nevertheless, the bones that also have high fracuture risks such as the spine and the proximal femur are covered with thick soft tissue. However, the single element transducer is not sensitive to the tissue thickness as well as the volume of the cancellous bone at the central skeleton sites. Therefore, the B mode ultrasound which uses array probes could help solve the problem. And this feature is helpful for the signal selection of the bone backscatter as

well as the attenuation compensation distance of the soft tissue. Therefore, the backscatter coefficients from three ultrasound probes are studied in order to see the accuracy of the correlation with the trabecular thickness, trabecular spacing and the BV/TV.

3.2 The Geometry of Ultrasound Probes

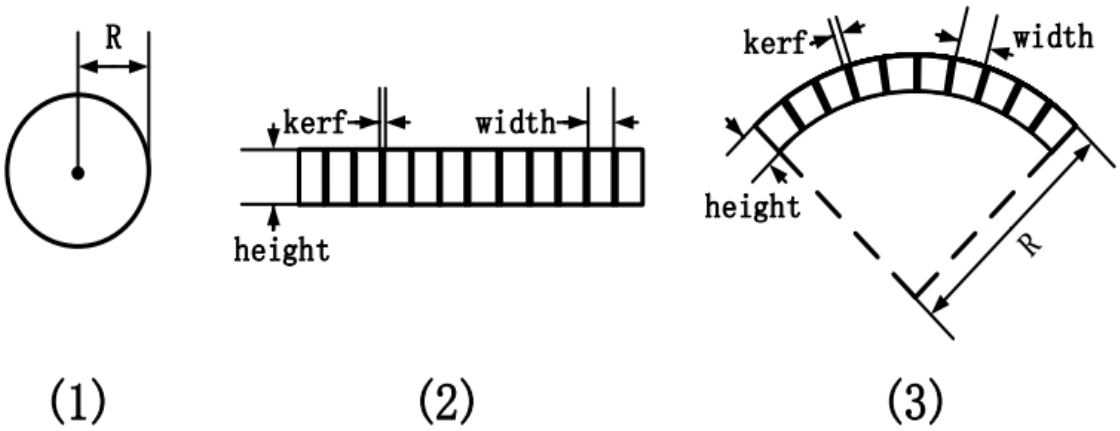

FIGURE 3.1: *The Properties of the Ultrasound Probes:(1) is the single element probe, (2) is the linear array probe and (3) is the curved array probe.Kerf is the space between two piezo-electric transducer elements*

The ultrasound probes could be divided into three categories: single probes (Fig. 3.1), also known as the single element probes; 1D probes (Fig. 3.2), which include the linear array probes and the curved array probes ; 2D probes which is applied to obtain 3D image. The single element probes may contain two transducers, each for ultrasound signal transmission and each for receive. And also the single transducers that combine both transmit and receive are available. The single element probes are widely applied in industry, for measuring metal thickness and detect lesion. The 1D and 2D probes are mainly used in the medical field, especially in obstetric ultrasonography.

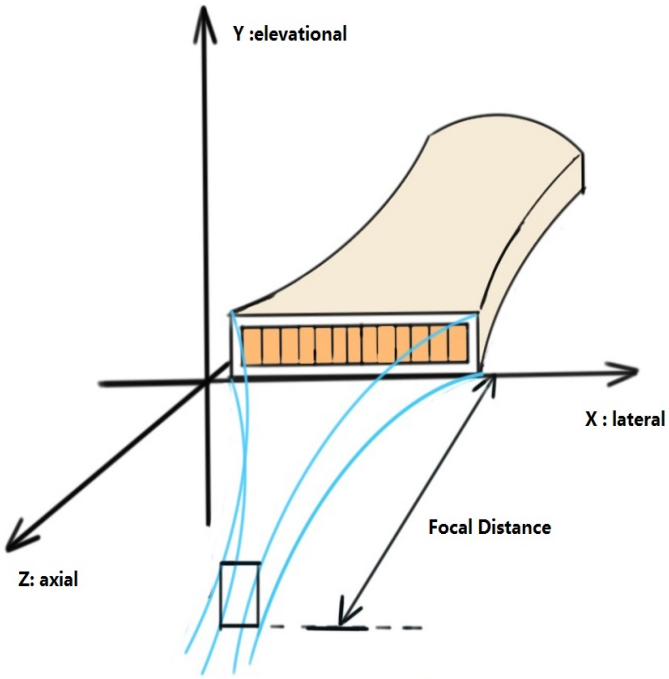

FIGURE 3.2: *The Linear Array Probe and the Focal Zone*

3.3 The Simulation Study using three Probe Models

The Property of the Bone Model

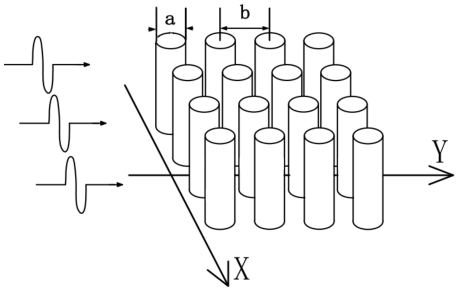

FIGURE 3.3: *The Cylindrical Bone Model*

The cylindrical array model (Fig. 3.3) was used in the simulation study [94]. The bone model was composed of uniform size cylinders with diameter of "*a*" and spacing of "*b*". The height of cylinders is 4mm, which is supposed to be long when compared with the height of transducer beam . 24×24 cylinders on X and Y axis were built and cylinders

were oriented perpendicular to the propagation direction of ultrasonic wave.The simulation was performed using a software named FOCUS (http://www.egr.msu.edu/∼fultrasweb/).

Three bone model groups with microarchetecture variation were simulated. (1) "*a*" (0.18 mm); "*b*" (0.69-0.85 mm) [32] with step increase of 1.6×10^{-5} mm. (2) "*b*" (0.69 mm); "*a*" (0.18-0.15 mm) with step increase of -3.0×10^{-6} mm. (3) combined variation group, "*a*" (0.18-0.15 mm) with step increase of -3.0×10^{-6} mm; "*b*" (0.69-0.85 mm) with step increase of 1.6×10^{-5} mm. For each model, the simulation was repeated 10 times with step movement of "*b*" $\times 10^{-1}$ on the x-axis. 20 groups of radio frequency data from the center elements of probes which covered the bone model surface area were obtained for calculation. The reference signal was from a planar model. The beamforming technique is dynamic focusing.

The Properties of the Transducer Models

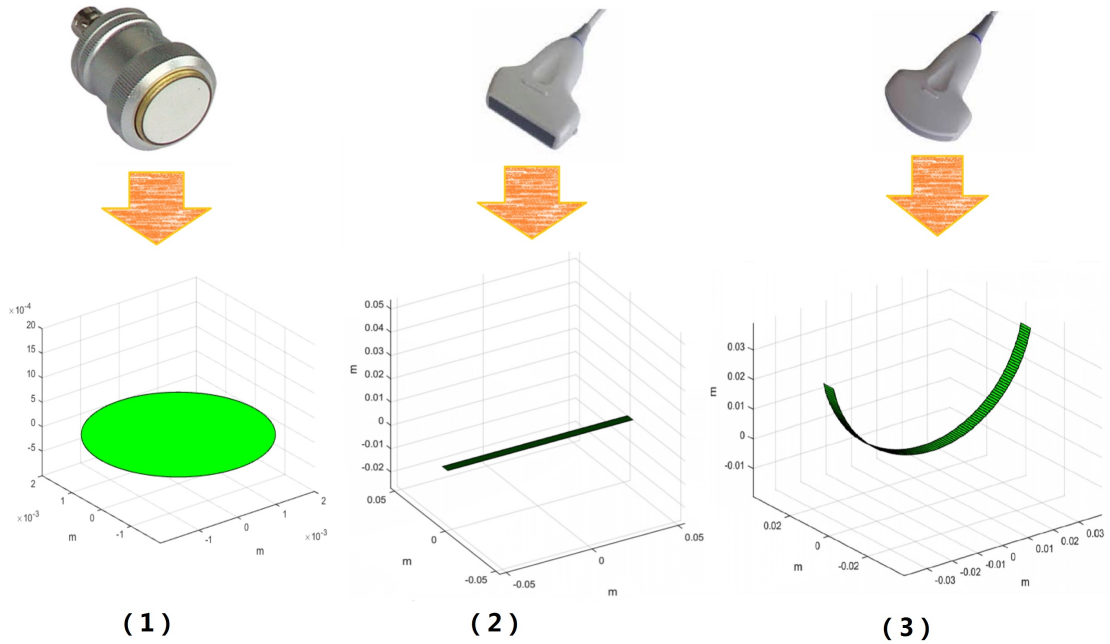

FIGURE 3.4: *The Simulation Models of Three Transducers*

Three transducer models (Fig. 3.4) were built in this simulation :(1) The single transducer (radius 2mm), (2) the linear array transducer and (3) the curved array transducer .

The parameters of transducers are listed in Table 3.1. The central frequency of transducers is 2MHz. The geometrical prototype of the curved array transducer is from a clinical probe (L12-5 38mm, ATL, Bothell, Washington), and for the linear array transducer is from a convex probe (C5-2 40R, ATL, Bothell, Washington) . Other geometrical features are from [68].

TABLE 3.1: *Multi-element Probe Parameters*

Element	**Number**	**Kerf**	**Width**	**Height**	**Radius**
Linear	128	0.1mm	λ	4mm	$--$
Curved	128	0.1mm	λ	4mm	4cm

The Calculation of the Backscatter Coefficient

The Backscatter Coefficient is expressed as:

$$\mu_B(f) = 8.68ln\frac{\langle S_B(f)\rangle}{S_0(f)}A(f)V(f) \tag{3.1}$$

Where $\langle S_B(f)\rangle$ is the backscattered spectrum, $S_0(f)$ is the reference spectrum from a perfect reflecter. $A(f)$ stands for attenuation compensation and $V(f)$ stands for volume compensation, including compensation for Hamming gate function, attenuation path and transducer geometry. The attenuation compensation and volume compensation is from Chaffai's work [43], and the detail is in Eq. 2.5 and Eq. 2.6.

The Calculation of Porosity

Porosity is the left ratio of bone material volume (BV) over bone tissue volume (TV) [69]. It could be expressed as (Eq. 3.2):

$$Porosity : P = 1 - BV/TV \tag{3.2}$$

In the cylindrical phantom, the bone material volume stands for volume of cylinders. Therefore, (Eq. 3.2) is equal to (Eq. 3.3) :

$$Porosity : P = 1 - \pi a^2 / b^2 \tag{3.3}$$

3.4 The Simulation Result and Discussion

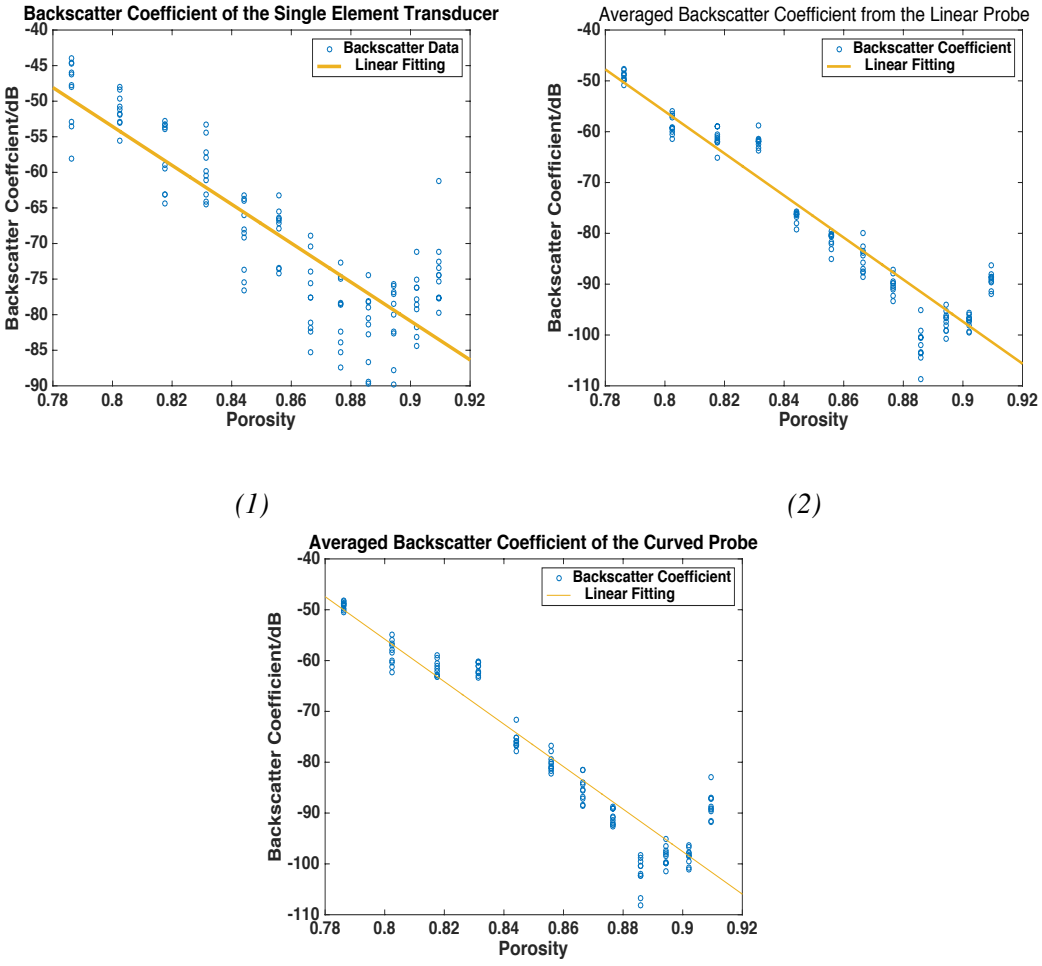

FIGURE 3.5: *The Correlation of the Backscatter Coefficient from Three Ultrasound Probe Models with the Porosity of group 3:(1) is the backscatter coefficient from the single element transducer, (2) is the backscatter coefficient from the linear array transducer, (3) is the backscatter coefficient from the curved array transducer.*

TABLE 3.2: *The Absolute Correlation Coefficients between Backscatter Coefficients and the Porosity*

Group	Single Transducer	Linear Probe	Convex Probe
(1)	$R: 0.97^{**}; SD: 10.05$	$R: 0.88^{*}; SD: 7.39$	$R: 0.84^{*}; SD: 7.02$
(2)	$R: 0.77^{*}; SD: 8.64$	$R: 0.96^{**}; SD: 8.48$	$R: 0.97^{**}; SD: 7.50$
(3)	$R: 0.94^{**}; SD: 10.84$	$R: 0.92^{*}; SD: 6.60$	$R: 0.95^{**}; SD: 6.89$

$*$ for p$<5\times10^{-2}$,$**$ for p$<1\times10^{-4}$, *SD* for Standard Deviation

The Backscatter Coefficient from the single-element transducer , the linear array probe and the curved array probe was calculated using Eq. 3.1. The Pearson correlation coefficients (R) between analytical and simulated results were calculated as in Table 3.2. BSCs of the single transducer correlated better with the change of Tb.Sp but less with the change of Tb.Th than multi-element probes. When the change of Tb.Sp and Tb.Th are combined, the correlations were similar. We further tested the single transducer with various radius (0.5-5mm), the correlation range in group (1) was 0.94-0.97 and in group (2) was 0.60-0.89. The SD indicates that the robustness from both multi-element probes were better than the single transducer.

3.5 Conclusion

In conclusion, BSCs from all three transducers were highly correlated with theoretical results but the array probes showed less stardard deviation. When measuring the backscatter coefficient in the in vivo experiment, the backscattered spectrum from different sites of the bone are collected in order to get an averaged backscatter coefficient that present the porosity of the whole bone. [40] The single element transducer, which showed larger standard deviation of the backscatter coefficient, may result from the narrower focal zone when compared with the array probes. The 1D array ultrasound probe are more likely to present more accurate backscatter coefficient in the region of interest. These results may contribute to the future development of a 1D ultrasonic tool using backscatter

for bone assessment. An in vitro study in Chapter 5 is followed by this study.

Chapter 4

A Quantitative Ultrasound Backscatter Measurement for Fetal Femur Bone Density Evaluation: A Simulation Study based on the Biot's Theory

4.1 Introduction

Antenatal screening has proven to be an effective way of monitoring fetal growth, assessing fetal well-being and for the early detection of fetal anomalies. For clinical purposes the modality of choice has been ultrasound with an excellent track record as a safe and non-ionizing way to monitor the fetus throughout pregnancy. Routine ultrasound parameters to monitor fetal development include femur length (FL), biparietal diameter (BPD) and head circumference (HC), which also allow the calculation of fetal weight estimates [70]. Currently there are no non-ionizing methods available for assessment of fetal bone density except MRI. However, the MRI is noisy and the scanning time is long (20-45 mins). What's more, the fetal movement would bring artifact to the image which might lead to inaccuracy. A new non-onizing method would be highly desirable, as fetal bone density not only reflects current fetal bone health but also has implications in the context of developmental programing, projecting bone health into adolescence and

adulthood [71]. There are multiple factors that impact on fetal bone density such as the maternal nutritional status [72], hormonal factors as well as mechanical stress [23]. Hence, fetal bone density can potentially guide interventions and preventive measures to improve long term health outcomes. Therefore, to solve this problem our approach explores the possibility of using ultrasound to determine fetal bone density during routine antenatal ultrasound investigations.

Current ultrasound methodologies available for bone density detection of neonates is to use a pair of ultrasound probe which clamps on the arm of the baby as transmit and receive to measure the speed of sound and ultrasound attenuation [8, 73, 74]. And a single probe which incorporated the transmit and receive transducers is also available [9]. Nevertheless, these methods are not applicable for fetal bone density evaluation. Because the transmit-receive method is not accessible for fetal bones, and the interference from maternal bone and tissue, the change of fetal bone location caused by fetal movement, making the transmit-receive method more difficult. Ultrasound backscattering based on the array probe, which only uses a single probe to measure the backscattered signal, is more accessible to the fetal femur. And it could provide B-mode images that could help locate the bone and measure the thickness of maternal tissue, which is useful for signal compensation.

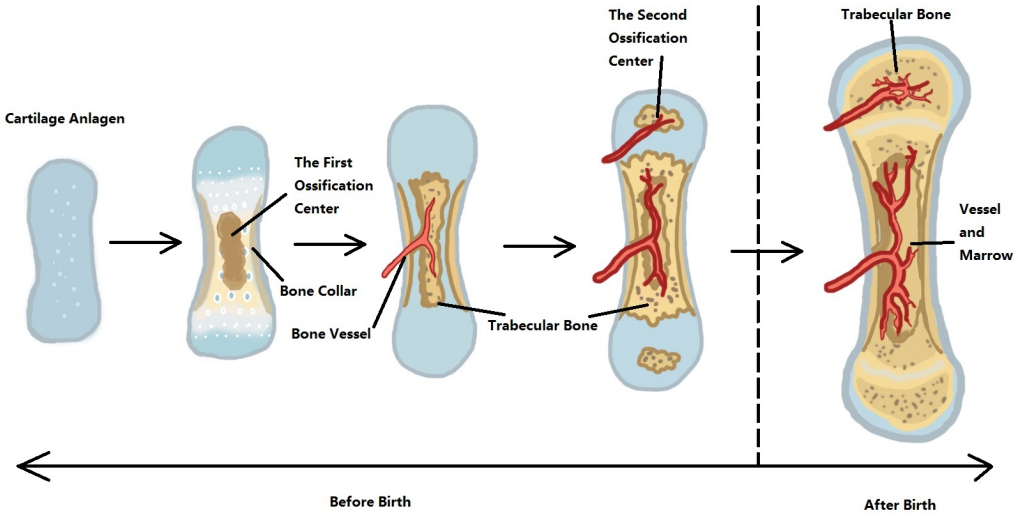

FIGURE 4.1: *The Development of Fetal Femur*

The ossification process of the prenatal femur bone is summarized as follows: As in Fig. 4.1 [10] the bone development starts with the of limb buds, after 6-9 weeks, the cartilage anlagen of long bone are developed. Then the bone collar starts to show at the central shaft which becomes the center of the first stage ossification [31]. The collar prevents the absorption of nutrition in the center and this results in a cavity, this cavity is then occupied by blood vessels. So the ossification area expands towards the ends of the long bone. In the last stage of prenatal bone development, the center of the secondary ossification is formed at the end of the bone. The secondary ossification starts from 2-4 months after birth, and the ossification at proximal epiphysis and the greater trochanter is developed [23].

In this paper, we used the Biot poroelastic model to simulate the biomechanical feature of the fetal cancellous femur. The Biot model is applied to study the ultrasound wave properties in the cancellous bone before, such as ultrasound velocity [75], attenuation [76] and scattering [77]. Fellah et al. [78] proposed a method to obtain the transmission and reflection coefficient in both the frequency and time domain.They further studied the impact of Biot parameters such as Bulk modulus and tortuosity to the amplitude of reflected signal [79]. Buchanan et al. [80] proposed a transfer function in cancellous bone. Nguyen et al. [81] did a transient simulation of ultrasound propagation in cancellous bone, they proposed a novel method to compensate the inclination of bone sample. Other studies also successfully applied Biot model to geometrical sediment study [82, 83]. A review of Biot theory in cancellous bone is available in [84].

The contribution of this work is that :(1) To our knowledge, this is the first model that proposed for fetal bone density evaluation using B-model ultrasound system. (2) An attenuation compensation methodology was proposed based on the abdomonal tissue thickness, distance of amniotic fluid and fetal femur tissue thickness measured by B-model ultrasound images. (3) The simulation results was compared with theoretical reflection coefficient from the Biot's theory, a good correlation and small standard deviation was found. This result shows that the backscatter coefficient from the fetal bone is able to provide bone density information.

4.2 Methodology

The Biot's poroelastic Theory

The equation of Biot's poroelastic waves that represent motion of solid frame and the fluid is [85, 86]:

$$\rho_{av}\frac{\partial^2 \boldsymbol{\mu}}{\partial t^2} + \rho_f \frac{\partial^2 \boldsymbol{w}}{\partial t^2} - \bigtriangledown \cdot \sigma = 0 \tag{4.1}$$

$$\rho_f \frac{\partial^2 \boldsymbol{\mu}}{\partial t^2} + \frac{\mu_f}{\kappa}\frac{\partial \boldsymbol{w}}{\partial t^2} + \frac{\tau \rho_f}{\varphi}\frac{\partial^2 \boldsymbol{w}}{\partial t^2} + \bigtriangledown p_f = 0 \tag{4.2}$$

Where $\boldsymbol{\mu}$ is the displacement of the solid material, $\boldsymbol{w}$ is the displacement of the fluid. σ is the total stress tensor. ρ_f is the density of fluid, ρ_s is the density of solid, φ is the porosity. ρ_{av} is the average density within the sample, therefore $\rho_{av} = \varphi * rho_f + (1 - \varphi) * rho_s$. μ_f is fluid viscosity, κ is the permeability and τ is the tortuosity.

The Biot-Willis elastic constants which are related to sediment bulk modulus of the solid, fluid frame and porosity are :

$$P_{biot} = \frac{(1-\varphi)(1-\varphi-\frac{K_b}{K_s})K_s + \varphi\frac{K_s K_b}{K_f}}{(1-\frac{K_b}{K_s}) - \varphi(1-\frac{K_s}{K_f})} \tag{4.3}$$

$$Q_{biot} = \frac{(1-\varphi-\frac{K_b}{K_s})\varphi K_s}{(1-\frac{K_b}{K_s}) - \varphi(1-\frac{K_s}{K_f})} \tag{4.4}$$

$$R_{biot} = \frac{\varphi^2 K_s}{(1-\frac{K_b}{K_s}) - \varphi(1-\frac{K_s}{K_f})} \tag{4.5}$$

The reflection coefficient $R(w)$ is given as :

$$Rco(w) = \frac{F_4^2 - 1 - F_3^2}{F_3^2 - (1 - F_4)^2} \tag{4.6}$$

$$F_i = \frac{2k_i\psi_i}{k\psi sinh(jk_iL)}(1 - \varphi(1 - \mu_i))\rho_f s^2, i = 1,2 \tag{4.7}$$

$$F_3 = \sum_i F_i, F_4 = \sum_i F_i * cosh(jk_iL) \tag{4.8}$$

Where ki is the propagation constants of fast and slow wave, μ_i is the amplitude of displacement for fast and slow waves. k is the wave number, ki are the constants of fast and slow waves, $i = 1,2$. ψ, ψ_i and s are intermediate values. The details of the reflection coefficient from the Biot's theory are in the [78, 79].

The pulse from the ultrasound transducer

The sine wave pulse (Fig. 4.2) in function Eq. 4.9 was generated from 128 elements of the ultrasound curved probe with central frequency of 2MHz [81] (Fig. 4.6). We could see the acoustic wave from the boundary of soft tisse and amnionic fluid , and two backscatter waves from the two boundaries of the fetal femur bone in Fig. 4.7. The signal received from the transducer elements that in the femur region was captured for signal processing.

$$P_{in} = 100 * e^{-4(f_0 t - 1)^2} sin(2\pi f_0 t) \tag{4.9}$$

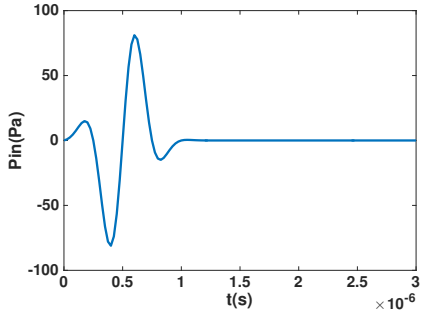

FIGURE 4.2: *The Pressue Pulse from the Transducer Elements*

The Proposed Backscatter Coefficient for Fetal Bone Density Evaluation

The backscatter coefficient from an array probe is as below [87, 88]:

$$BSC_{array} = V_{com} * A_{com} * \frac{\gamma^2}{4} * \frac{1}{N} * \sum_{N}^{i=1} \frac{S_i(f)}{S_{ref}(f)} \tag{4.10}$$

Where V_{com} is the compensation of beam volume based on the shape and focus point of the transducer. A_{com} is the compensation for the attenuation during wave propagation and hamming gate. N is the number of transducer elements. $S_i(f)$ and $S_{ref}(f)$ are the power spectrum from the bone and the reference material (a steel plate as the perfect reflecter), respectively.

The compensation of beam volume is given as :

$$V_{com} = \frac{3d^2R^2}{2w^2LA'} \tag{4.11}$$

Where d is the element center-to-center distance, w is width of the element, R is the focal distance, L is the gated signal length, A' is area the of transducer aperture.

The attenuation compensation is :

$$A_{com} = A_{path}(\frac{2\alpha f_0 L}{1 - e^{-2\alpha f_0 L}})^2[1 + (\frac{2\alpha f_0 L}{2\pi})^2]^2 \tag{4.12}$$

The proposed tissue attenuation compensation during ultrasound wave propagation :

$$A_{path} = e^{4(a_{at}x_{at}+a_{aw}x_{aw}+a_{ft}x_{ft})} \tag{4.13}$$

$$\alpha = \frac{1}{8.686} * \frac{10}{L} * ln\frac{S_{ref}(f)}{S_{bone}(f)} \tag{4.14}$$

In Eq. 4.13, α is the backscatter attenuation coefficient (Np/cm) of the femur bone, which is the natural logarithm ratio of the backscattered reference power intensity devide by bone power intensity in the gated region and L is in cm (Eq. 4.14, Fig. 4.9). $S_{bone}(f)$ is the spacial averaged spectrum of $S_i(f)$.

In Eq. 4.13, A_{path} is the round-trip frequency-dependent attenuation compensation during the propagation path before reaching femur bone. The advantage of the B-mode ultrasound is that it is able to measure the thickness of the tissue. Therefore, x_{at} is the averaged thickness of abdominal tissue. x_{ft} is the thickness of the femur tissue. x_{aw} is the distance of amnionic fluid. a_{at}, a_{aw} and a_{ft} are the empirical attenuation coefficient of abdominal tissue, amnionic fluid and femur tissue,respectively. In addition to the backscatter coefficient, the AIB which does not need attenuation compensation is bone was also calculated.

$$AIB = \frac{1}{f_{max} - f_{min}} \int_{f_{min}}^{f_{max}} 8.68 ln(A_{path} * V_{com}(f) * \frac{1}{N} * \sum_{N}^{i=1} \frac{S_i(f)}{S_{ref}(f)}) df \tag{4.15}$$

The Theoretical Backscatter Coefficient from the Biot's Model

The calculation of theoretical reflection coefficient was based on the Table 4.1 and Eq. 4.6- 4.8, in which the parameters were from in vitro experiment of human femur [89]. The correlation between the theoretical reflection coefficient and bone porosity is in Fig. 4.3.

TABLE 4.1: *Biot-Stroll Model Parameters*

Name	Parameter	Value	Name	Parameter	Value
Central Frequency	f0	2 MHz	Speed of Sound	c0	1540 m/s
Porosity	φ	0.5-0.95	Permeability	κ	3.6e-6 cm^2
Fluid viscosity	μ_f	1e-3 $Pa \cdot s$	Fluid density	rhof	$1000 kg/m^3$
Bulk modulus of solid frame	Kb	0.67 GPa	Solid density	rhos	1800 kg/m^3
Bulk modulus of grains	Ks	10.8 GPa	Drained density	rhod	$rhos * (1 - epsilonP)$
Shear modulus of solid frame	G	0.42 GPa	Pore size	p_{size}	0.5e-3 m
Bulk modulus of fluid	Kf	$rhoF * c0^2$ GPa	Tortuosity	τ	1.5

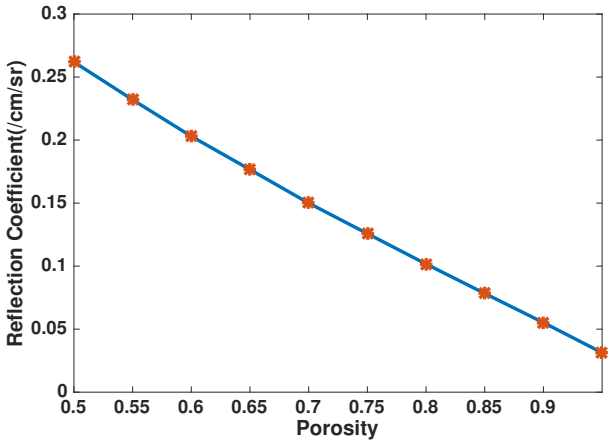

FIGURE 4.3: *Correlation between the Theoretical Reflection Coefficient and the Bone Porosity*

The Simulation of the Fetal Femur Model

Comsol (COMSOL Incorporation,Burlington, MA, USA) is selected as the tool for the simulation study. The model (Fig. 4.5) is based on the actual size of fetal femur bone in the third trimester. Fig. 4.4 is the B-mode image of a fetal femur (The usage of the figure is approved by Nepean Blue Mountain Local District Human Research Ethics Committee (EC00151)). For gestational ultrasound diagnosis, the curved array transducer is applied

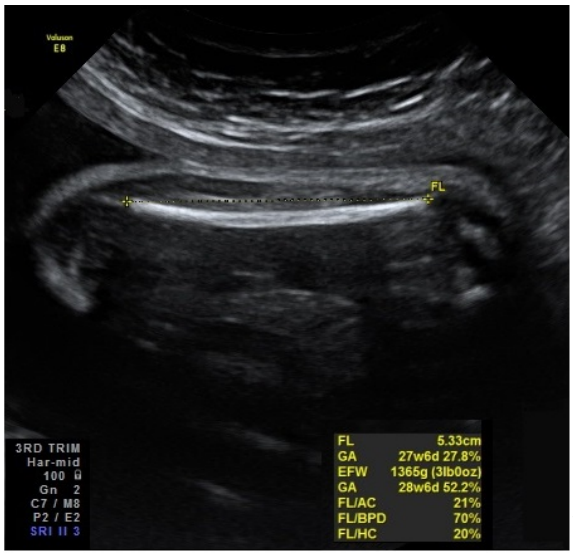

FIGURE 4.4: *B-mode Ultrasound Image of Fetal Femur from a Clinical Study*

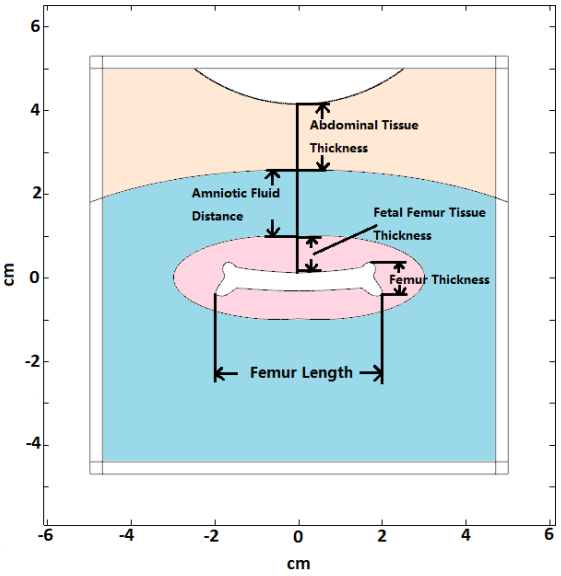

FIGURE 4.5: *Simulation Model of Fetal Femur*

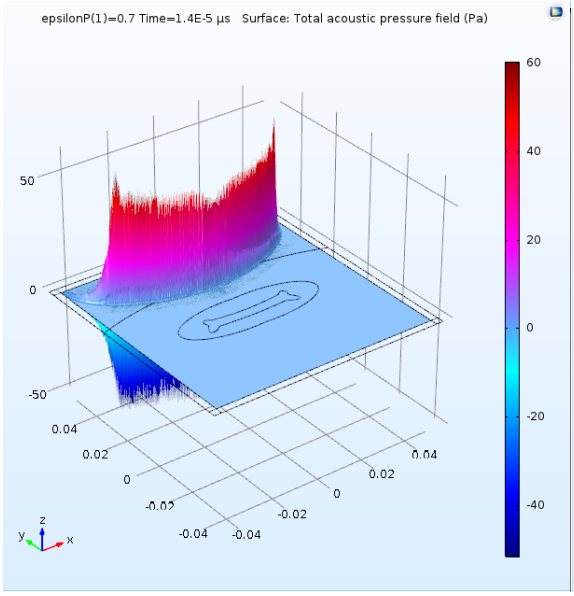

FIGURE 4.6: *The Wave from the Transducer Elements*

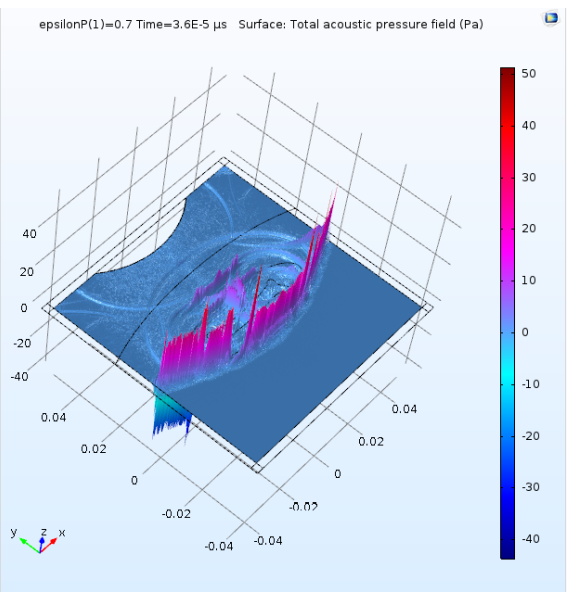

FIGURE 4.7: *The Backscattered Wave from Femur*

because the shape contacts well with abdominal skin and could provide a broader view of the B-mode image. Along the propagation way of ultrasound, the wave first passes through belly tissue, placenta, amnionic fluid, fetal femur soft tissue and finally reaches the femur bone. Therefore, in the fetal femur bone evaluation, proper compensation for

the attenuation during the transmission path is crutial for accurate backscatter measurement.

The size of the fetal femur and the thickness of the abdominal tissue are from literature. The fetal femur is set as poroelastic material. In the third trimester, the thickness of abdominal tissue ranges from 1-4.1 *cm* with average value of 2.16 *cm* [90], the average attenuation coefficient of the tissue including placenta is 0.47 $dB/(MHz*cm)$. The average fetal femur tissue thickness is 1.4 *cm* [91]. The femur bone length range is 6.0-7.9 *cm* [92]. The thickness ranges from 0.8 to 1.025 *cm*, which is interpolated from [93]. The average path length of amniotic fluid is 2.0 *cm*, with range from 0.5 to 4.3 *cm* [90]. The geometrical features of this model is listed in Table 4.2.

TABLE 4.2: *Geometrical and Acoustical Properties of Fetal Femur Model*

Parameter Name	**Parameter**	**Value**
Speed of sound in tissue	s_t	$1590m/s$
Average density of Tissue	rhot	$1000kg/m^3$
Thickness of abdominal tissue	x_{at}	1.7-2.2cm
Thickness of femur tissue	x_{ft}	0.9-1.3cm
Thickness of fetal femur	x_{fe}	0.8-1 cm
Length of fetal femur	l_{fe}	5.5-7cm
Attenuation Coefficient of abdominal tissue	a_{at}	0.47 $dB/(MHz*cm)$
Attenuation Coefficient of femur tissue	a_{ft}	0.53 $dB/(MHz*cm)$

The gated signal is selected 1us after the maximum of the backscatter signal (Fig. 4.8) to remove the noise from specular reflection. The power spectrum of the bone backscatter and the reference signal is in Fig. 4.9. 30 groups of data with various abodominal thickness, femur tissue thickness and distance of amniotic fluid were collected for signal processing.

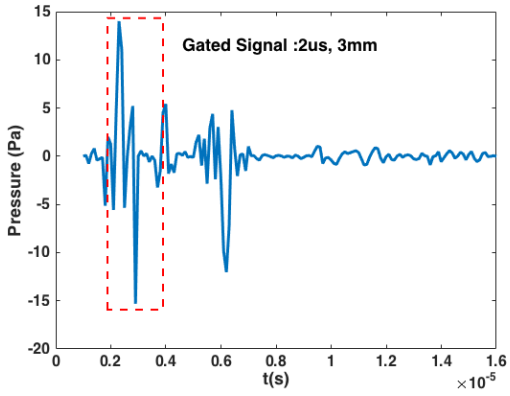

FIGURE 4.8: *The Gated Backscatter Signal*

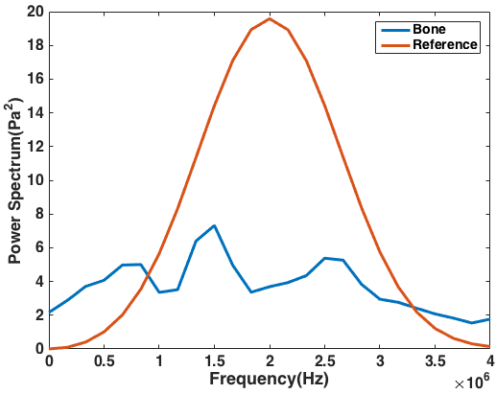

FIGURE 4.9: *The Power Spectrum of the Backscatter Signal*

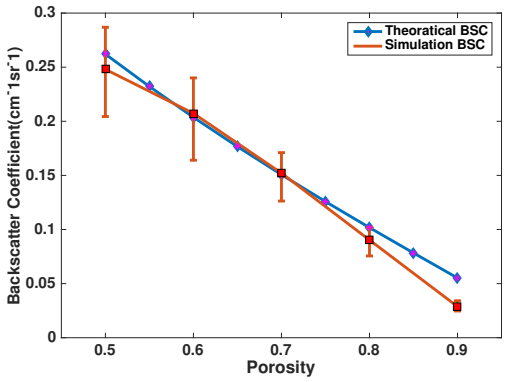

FIGURE 4.10: *The Correlation between Backscatter Coefficient and Porosity*

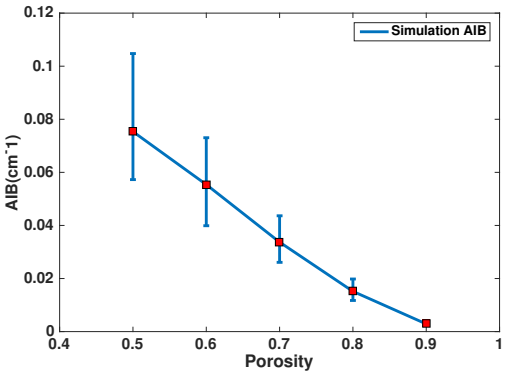

FIGURE 4.11: *The Correlation between Apparent Integrated Backscatter and Porosity*

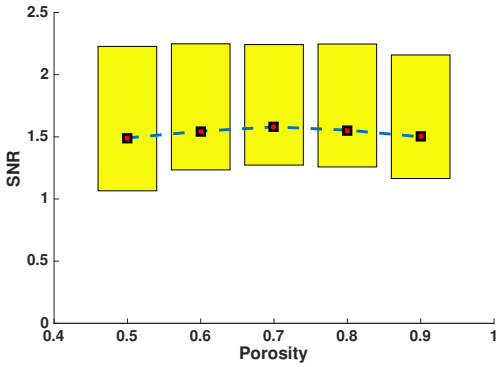

FIGURE 4.12: *The Signal to Noise Ratio*

4.3 Results

The Pearson correlation coefficient between the porosity with the backscatter coefficient and spectral centroid shift were calculated using Matlab. For backscatter coefficient, $R = -0.9970, P = 2.0058e-04, SD = 0.1021$ (Fig. 4.10), as for Apparent Integrated Backscatter, $R = -0.9469, P = 0.0146, SD = 0.1062$ (Fig. 4.11). The backscatter coefficient was also compared with the theoretical backscatter coefficient, and the correlation between the theoretical BSC and simulated BSC is $R = 0.9925, P = 7.8479e-04$. A highly significant correlation was found with the porosity and BSC as well as with the porosity and AIB, but the standard deviation of AIB is larger. These results indicate that after proper compensation during the ultrasound propagation in the soft tissue, the result from BSC and AIB are highly correlated with bone porosity. Ultrasound BSC and AIB may be accurate parameters to interprete bone density if consider the bone density as the average of the bone mass and tissue mass ($BMD = Porosity * \rho_{tissue} + (1 - Porosity) * \rho_{bone}$).

The signal to noise ratio was calculated based on the -3dB power spectrum selected and the noise out of the signal of interest. The result of each group is in Fig. 4.12 , and all the SNR is larger than 1 which indicate that the signal selected is of good quality.

4.4 Discussion

In this simulation study, the ultrasound backscattered data was adopted for fetal bone density evaluation. During the gestation period, the fetal development including the skeleton development is very sensitive to the external factors and the maternal environment, therefore ultrasound was chosen for its non-ionizing nature. The difficulty of fetal bone density evaluation includes :(1) The ultrasound would attenuate during propagation in the soft tissue and amniotic fluid, and this needs proper compensation. (2) The location of the fetal femur, and the thickness of the abdominal tissue, fetal tissue and amniotic fluid

varies in every pregnant women, and the fetal movement makes the evaluation more difficult. (3) The density of fetal femur is not homogenous, interference from collar bone and cartilage may affect the accurracy. (4)The spectrum power of the backscatter is not only related with the bone density, but also related to the bone volume of the region of interest. Use of only a single transducer might lead to inaccuracies because it has no access to the gated bone volume. Therefore, the B-mode ultrasound system, which is widely applied for fetal diagnosis in the second and the third trimester was chosen for its flexibility and visualization to fetal femur.

The result of the study showed a similar correlation trend with the BSC from [14, 39, 40, 44] (f0=0.5-1MHz, R=0.5-0.94) and AIB from [50, 52–55] (f0=0.5-5MHz, R=0.51-0.904). Compared with the those studies, this study achieved better results and the reason might be the smaller interference from the noise in the simulation study rather than in vitro or in vivo study. The related research that used the ultrasound imaging modality is from Zhang et al. [48] and Conversano et al. [47]. In Zhang's study they measured BSC from the neonates' femur and correlated BSC with the gestational age (R=0.47), birth weight (R=0.47) and length at birth (R=0.43). In Conversano's study, the region of interest is human spine and they achived significant correlation with the proposed osteoporosis score (R=0.859) and the DEXA result (R=0.866). The reason for the medium correlation in the Zhang's study may be that they did not correlate the BSC with the DEXA result, and the attenuation during the wave propagation might cause the inaccuracy. Conversano's work is more close to our study, they excluded the data when the spine is not properly located in the ultrasound beam region and they also proposed the gated signal volume compensation and the attenuation compensation during the transmittion path. Therefore, the result indicates that the BSC from the array transducer is possible to detect the bone mineral density and the compensation during the ultrasound propagation and the selected signal volume is neccessary to achive good correlation.

Except for the Biot model used in this study, there are other three models proposed for ultrasound backscattering in the cancellous bone : the Farran cylinder model, the weak scattering model and the binary mixture model [94]. The Farran cylinder model assumes

that the structure of the cancellous bone is composed of multiple identical cylinders, and the phase of the backscatter signal distributed uniformly from 0 to 2π . In the weak scattering model, the autocorrelation function was obtained from the structural information from microCT scan. The binary mixture model, which is developed based on the Biot's theory, it proposed that the backscatter coefficient is based on the mean fluctuation of the bone density and the velocity. Compared with other three models, the biot model considered the absorption and relaxation effects from the two media: the bone tissue and marrow tissue. Unlike the Farran cylinder theory or the autocorrelation theory which considered the backscattering as the sum of the scattered signal from a single scatterers, the Biot's theory considers the wave propagation from the bone framework and marrow seperately. And this assumption of structure is more close to bone microstructure in reality.

The limitation of the simulation is that we modeled the fetal femur as a homogeneous Biot poroelastic model. However, like in Fig. 4.1, the fetal bone is not very homogeneous. In the third trimester the collar which will be developed into the cortical bone is ossified, the cancellous bone would appear close to the two ends of the femur. Therefore, this simulation model needs to be developed further to evaluate the average bone density of fetal femur. Another limitation is that the poroelastic parameters of the Biot model is from adult human femur, because the lack of data from previous studies, we are not able to find all the poroelastic parameters for the fetal bone model, and this might limit the result.

4.5 Conclusion

In this study , a fetal femur bone model was built based on the Biot's theory for bone density evaluation. The B-mode ultrasound, which is widely adopted in the clinical fetal bone length evaluation, was chosen as the methodology for backscattering signal collection. The correlation with the porosity from the backscatter coefficient ($R = -0.9970$, $P = 2.0058e-04$, $SD = 0.1021$) and apparent integrated backscatter ($R = -0.94694$, $P = 0.0146$, $SD = 0.1062$) were calculated, and the result agrees well with the theoretical BSC and the previous in vitro and in vivo studies. This study might be helpful for fast

and non-ionizing diagonisis for fetal bone density for clinical usage.

Chapter 5

A Comparison Study of Ultrasound Backscatter Measurement of Cancellous Bone using the Fundamental Backscatter and the Second Harmonics

5.1 Introduction

Bone Mineral density (BMD) is an importanct indicator of human health: for senior people, it predicts the potential of osteoporosis. As for the baby and young child, it indicates the level of nutrition and bone growth. Current widely applied methodologies for bone density evaluation are Dual-energy X-ray Absorptiometry (DEXA), Magnetic Resonance Imaging (MRI) and Quantitative Ultrasound (QUS). Compared with ultrasound, DEXA and MRI are non-portable and more expensive. The current QUS devices which use separate transmit and receive transducers are only applicable to peripheral sites such as arm and heel. It has limited access to central sites that have high fracture risks such as femur neck and spine. Ultrasonic backscatter, which uses a single transducer for both transmit and receive, is more flexible to measure bone density.

Ultrasound second harmonics has shown better axial and lateral resolution in ultrasound B-mode imaging and smaller side lobes in tissue harmonic imaging [95]. The

integrated backscatter coefficient from the second harmonics of myocardial tissue was found to be better than the fundamental backscatter by Beaver et al. [96]. However,to the best of our knowledge, there is no study about the ultrasonics second harmonics in cancellous bone. Therefore, it is interesting to compare the backscatter from the second harmonics with the fundamental backscatter and see which method works better in bone structure characterization.

5.2 Background on Second Harmonics

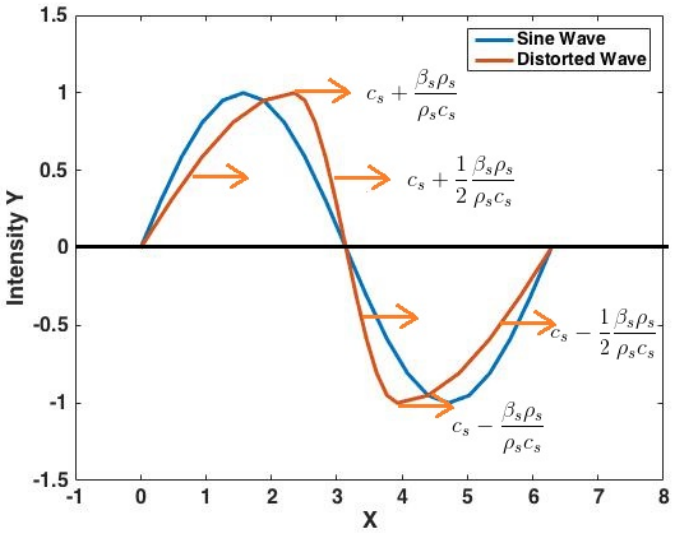

FIGURE 5.1: *The Distortion of the Sine Wave*

The nonlinear distortion of the sine wave as it propagates is the source for the generation of the second harmonics. As in Fig. 5.1, the sine wave with amplitude dependent phase speed is $c_0 + \frac{\beta p}{\rho_0 c_0}$, where c_0 is the speed of sound of the propagation medium, ρ_0 is the medium density, β is the coefficient of nonlinearity and p is the local acoustic pressure. The distortion results from the higher phase speed when $p > 0$ while the phase speed is slower when p is negative. The distortion leads to the spill over of power from the fundamental backscatter to the higher order harmonics. The power of harmonics increases with the signal propagation and the encounter with deeper inhomogeneous

tissue. The power of the second harmonics is typically 15dB lower than the fundamental backscatter [97].

The traditional way to obtain the second harmonics is to filter the signals around $2f_o$. However, because of the overlap between f_o and $2f_o$, the filtered signal is not able to achieve good performance in terms of contrast and resolution. Therefore, Simpson et al. [98] proposed a pulse inversion technique to obtain the second harmonics signal. The the second harmonics is obtained by the sum of the positive pulse and the inverted pulse, and the result showed that this technique is not only more sensitive to the nonlinear scattering, but also able to solve the problem of spectral overlap. The pulse inversion technique is now widely applied in commercial ultrasound systems.

In recent years, the bone density evaluation using backscatter images such as integrated backscatter image [34], AIB image [63] and SCS image [64] were investigated. Because the inhomogeneity and anisotropy property of the cancellous bone, these backscatter imaging techniques which covers wider spatial range are able to reveal more detailed structure information. However, early backscatter imaging methods adopted the time-consuming procedure to measure backscatter property at each image pixel with single element transducers. Later, the more convenient methods that uses the existing commercial ultrasound imaging systems to measure bone density were tested in vitro [99], on human spine [47], and neonates [48] and they achieved various success of the correlation between the bone mineral density. Therefore, in this study the ultrasound backscatter parameters BSC, AIB and SCS are measured using an ultrasound imaging system, and the result from both fundamental imaging and second harmonic imaging signal was compared. This study is a prerequisite study for the implementation of BSC in the commercial ultrasound imaging systems.

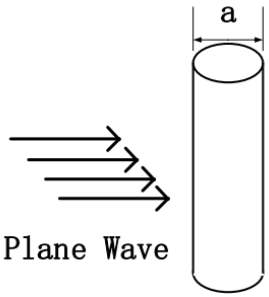

FIGURE 5.2: *The Cylindrical Model that Represent Trabeculae. "a" is the trabecular thickness*

5.3 The Fundamental Backscatter and the Second Harmonics from a Cylinder Model

The structure of the cancellous bone could be regarded as an interconnected bone frame that is filled with soft tissue such as fat and marrow. Trabeculae represent each of the microstructure of the bone frame. Wear et al. [38] proposed a Farran cylinder model (Fig. 5.2) to describe the intrinsic property of the backscatter from cancellous bone. They further claimed that this model could be applied to represent cancellous bone backscatter which has multiple cylindrical backscatter sources when given two conditions: (1) The cylinders are randomly distributed, and the backscattering phases are evenly distributed from 0 to 2π (2) Ignoring the multiple scattering effects.

To compare the ultrasonic backscatter of the cancellous bone from the fundamental backscatter and the second harmonics, we used the same cylinder model and calculated angular power distribution and the correlation between the trabecular thickness and the power spectrum. In Wear's work, they used the Farran cylinder model and while for the second harmonics, we calculated the backscatter from Abbasov et al. [100]. Both of the models assume that the backscatter is from the surface of a rigid cylinder.

The Ultrasound Fundamental Backscatter from the Farran Cylinder Model

The reflected power intenisty P_w from the Farran Cylinder Model is given as [38, 101]:

$$P_w = \frac{Ia}{2\pi r}|\varphi_s(\phi)|^2 \tag{5.1}$$

$$|\varphi_s(\phi)|^2 = \frac{1}{0.5 * ka}\sum_{m=0}^{\infty}\sum_{n=0}^{\infty}\varepsilon_m\varepsilon_n sin\eta_m sin\eta_n \times cos(\eta_m - \eta_n)cos(m\phi)cos(n\phi) \tag{5.2}$$

Where I is the intensity of the ultrasound wave, a is the diameter of the cylinder, r is the distance from the center of the cylinder to the observation point. ϕ is the angle between the propagation direction and the observation point, for backscattering $\phi = 180°$. $\varepsilon_0 = 1, \varepsilon_m = 2$ when $m > 0$. η_m is the phase angle.

$$tan\eta_n = tan\delta_n(x)\frac{tan\phi_n + tan\alpha_n(x)}{tan\phi_n + tan\beta_n(x)} \tag{5.3}$$

where $x = ka$, $tan\phi_n = 0$ for rigid cylinder, and

$$\delta_n(x) = tan^{-1}[-J_n(x)/N_n(x)] \tag{5.4}$$

$$\alpha_n(x) = tan^{-1}[-xJ'_n(x)/J_n(x)] \tag{5.5}$$

$$\beta_n(x) = tan^{-1}[-xN_n'(x)/N_n(x)] \tag{5.6}$$

Where J_m and N_m are Bessel and Neumann functions, respectively.

The Ultrasound Second Harmonics from the Cylinder Model

The power intensity of the second harmonics from the cylinder model is :

$$\begin{aligned} P_{2\omega} =& \frac{C_{2\omega}(1+isin\varphi)}{2ik_{2\omega}(cos\varphi+1)} \\ & \times [exp[ik_{2\omega}(cos\varphi+1)d] - exp[ik_{2\omega}(cos\varphi+1)\frac{a}{2}]] \\ & + \frac{C_{2\omega}(1+isin\varphi)}{2ik_{2\omega}(cos\varphi-1)} \\ & \times [exp[ik_{2\omega}(cos\varphi-1)d] - exp[ik_{2\omega}(cos\varphi-1)\frac{a}{2}]] \end{aligned} \tag{5.7}$$

$$K_{2\omega} = 2\varepsilon\omega_1^2\rho_0\psi_{10}^2/c_0^4 \tag{5.8}$$

$$C_{2\omega} = -exp(-ik_{2\omega}r)K_{2\omega}/\sqrt{2\pi k_{2\omega}r} \tag{5.9}$$

Where ε is the quadratic nonlinearity parameter, ω_1 is the wave frequency, a is the cylinder diameter, d is the quasi-diffraction distance, ρ_0 is the density of the surrounding medium, c_0 is the speed of sound in the medium, ψ_{10} is the amplitude of the velocity potential function, $k_{2\omega}$is the wave number of the second harmonics, r is the distance to the observation point.

The Comparison Between the Two Theoretical Models

We calculated the angular distribution of the scattering from the two theoretical cylinder models with the given parameters below:

TABLE 5.1: *Parameters for Theoretical Calculation*

Farran Cylinder		**2nd Harmonics Cylinder**	
Parameter	**Value**	**Parameter**	**Value**
I	1	ψ_{10}	1
a	0.075 (mm)	a	0.075 (mm)
r	2 (cm)	r	2 (cm)
c_0	1540 m/s	c_0	1540 m/s
$\varepsilon_m, \varepsilon_n$	$\varepsilon_0 = 1, \varepsilon_m = 2 (m, n > 0)$	ε	36 [102]
k	$2\pi f / c_0$	k_{2w}	$2\pi f_{2w} / c_0$
x	$x = ka$	ω_1	$2\pi f$
J_m	Bessel Function	r	0.02m
N_m	Neumann Function	ρ_0	1000 kg/m^3
$tan\phi_n$	0	ω_1	$2\pi f$
		d	20a

We assume that the central frequency is f=2MHz and the frequency of the second harmonics is $f_{2\omega}$=4MHz. The surrounding medium is water. With the parameters given as Table5.1, we are able to obtain the correlation of power spectrum $\left|P_{2\omega}^2\right|$ using a (0.15-0.18mm) from [32].

The angular distribution of backscatter power spectrum from the two theoretical cylinders was calculated with center frequency ranges from 0.5 Mhz to 7 Mhz (Fig. 5.3). The overall trend of the power spectrum change with the cylinder radius is in the Fig. 5.4.

The overall positive trend was found with the correlation between power spectrum and radius of the cylinder. And the angular distribution from the fundamental backscatter indicates that in the lower frequency(<2MHz), the scattering of the power spectrum is

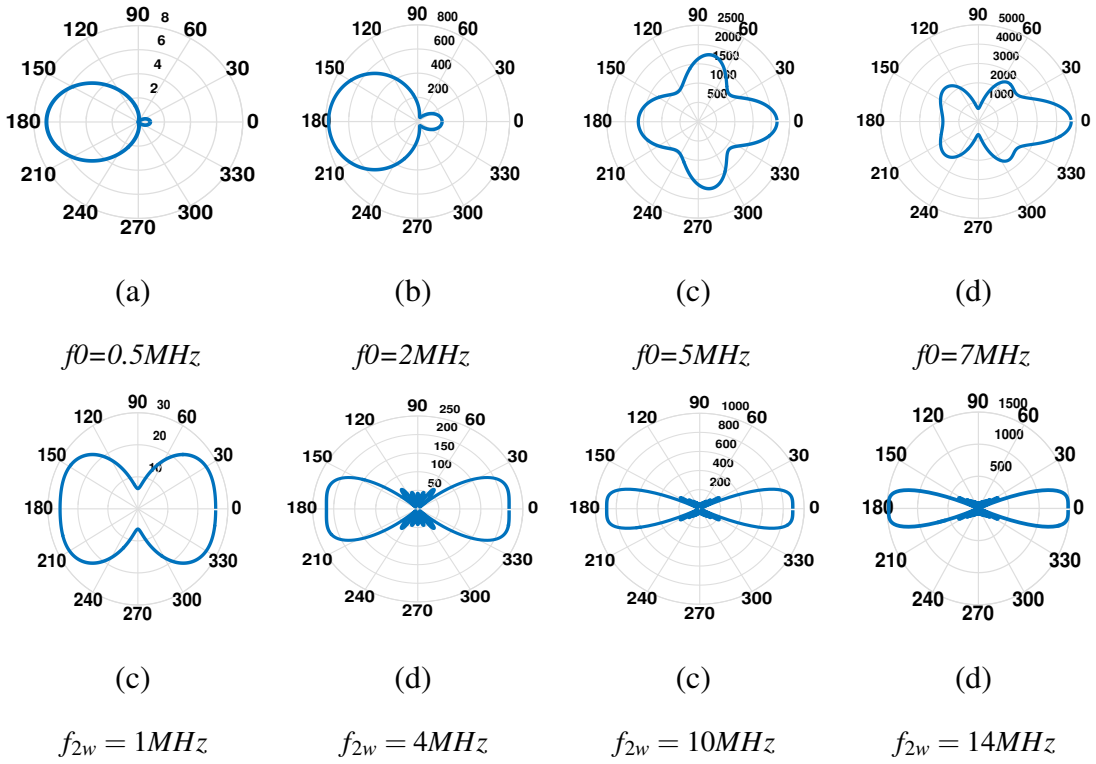

FIGURE 5.3: *The Angular Distribution of Scattering from the Surface of Two Cylinder Models. f0 is the central frequency, $f_{2\omega}$ is the 2nd harmonics. The reference pressure is from water 1u Pa*

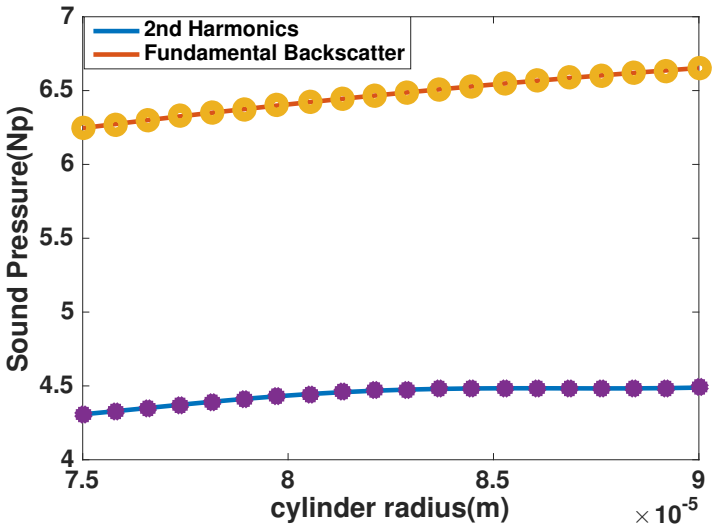

FIGURE 5.4: *The Correlation between the Sound Pressure of the Fundamental Backscatter and the 2nd Harmonics with the Change of Cylinder Radius.*

at the backscatter direction (180°). In the higher frequency (>5MHz), the power spectrum distributes at both the propagation direction (0°) as well as the backscatter direction (180°). As for the second harmonics, the power distribution is always at both the

propagation direction and the backscatter direction. The power spectrum distribution of two theoretical models are simular, and the backscatter power increases with the cylinder radius, which indicates that the backscatter increases with the trabecular thickness. This model can also describe the backscatter coefficient from multiple scatterers, if the scatterers are positioned sufficiently random and then the multi-scattering effect could be ignored [37]. However, this is a simplified theoretical model of the trabecular structure. An in vitro experiment was conducted to further study the correlation with BMD.

5.4 Methodology of the In Vitro Experiment

FIGURE 5.5: *The Prepared Bone Samples*

Bone Sample Preparation

50 cubic bone samples (Fig. 5.5) of bovine femur were prepared with an electrical saw. The average size of samples is: length (1.392±0.2435cm), width (1.2956±0.224cm), height (1.056±0.2481cm). Trichloroethylene (C_2HCl_3) was used to remove the fat and marrow in the bone samples. The samples were then preserved in the 0.9% saline at 20° temperature [40]. All the bubbles are removed before measurement.

Dual-energy X-ray Absorptiometry (DEXA) Scan

BMD data obtained from Dual-energy X-ray Absorptiometry (DEXA) scan was used as a gold standard for correlation calculation. The BMD data was obtained using Faxitron Ultrafocus DXA system. The exposure settings of properties are: Low Energy: 40kV, High Energy: 80kV, Tube current: 0.2mA, time:2.2s.

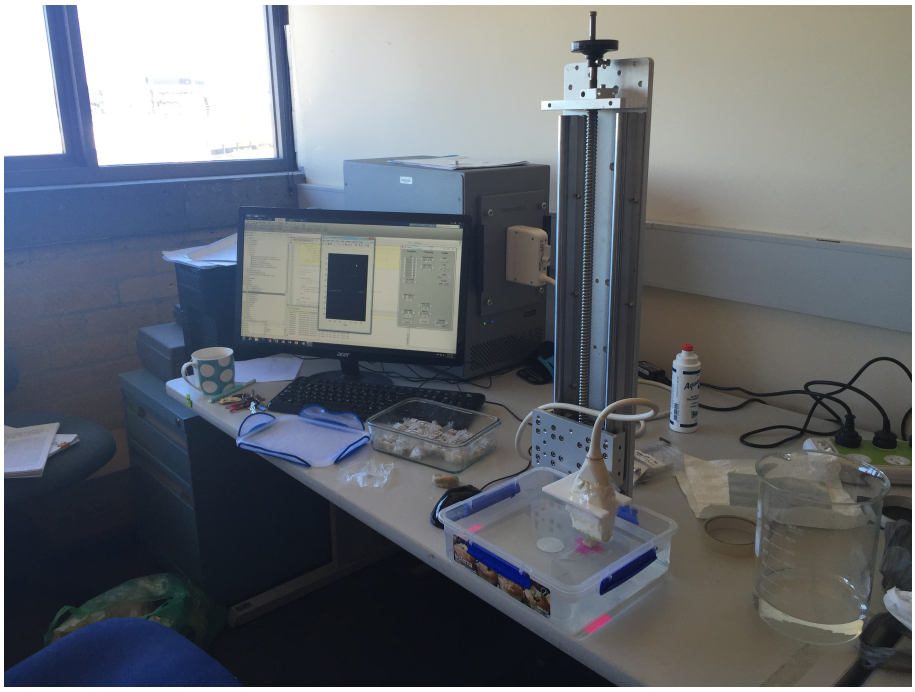

FIGURE 5.6: *The Backscatter Measurement of Cancellous Bone using an Ultrasound Imaging System*

Ultrasonic Measurement

The Vantage LE64 System was used to obtain ultrasound radiofrequency (RF) data. A curved array ultrasound probe (C5-2 40R, ATL, Bothell, Washington), with the central frequency of 2MHz was held with a 3D printed transducer holder and mounted on a linear rail (Fig. 5.6). The system is switched to pulse-echo mode with time gain compensation set as 0. The voltage for the fundamental backscatter is 20 Volts while for the 2nd harmonics is 40 Volts due to its high attenuation. 6 faces of the sample cube were measured both with first harmonic mode and second harmonic mode with 2cm distance to the transducer, and 5 groups of data from 300 sample faces were collected. The harmonic

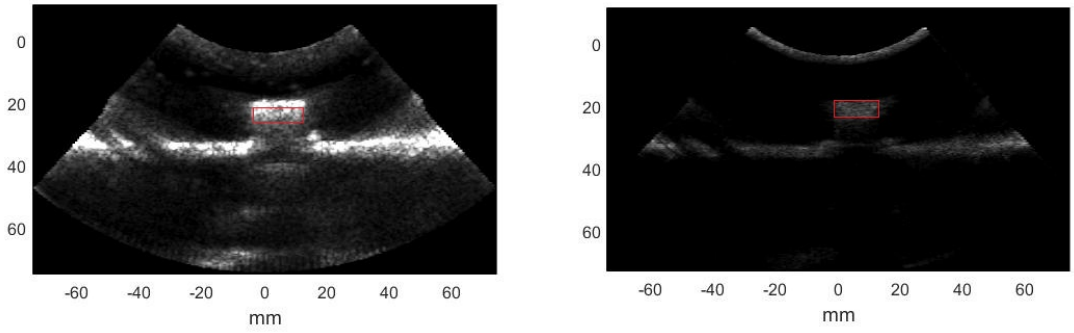

FIGURE 5.7: *The B-mode Ultrasound Images from the Fundamental Backscatter (left) and the Second Harmonics (right). The Selected Region is the Region of Interest.*

signal was captured by the standard pulse inversion technique, which was the sum of the positive and the reversed pulses.The reference signal is for the fundamental backscatter and the 2nd harmonics were measured seperately from a flat stainless steel sheet in both the fundamental mode and the 2nd harmonics mode.

Signal Selection

In this experiment, BSC, AIB and SCS were calculated. For the fundamental signal, the RF signals were first Hilbert transformed, then the signal was selected 1us after the peak of the envelope to exclude the interference from the specular echo. 2us data which present 3mm signal length was gated as the region of interest. For the 2nd harmonics, because there is less specular echo interference, the 2us data was selected directly after the peak of the envelope. The region of interest is in Fig. 5.7.

Calculation of Parameters

The Apparent Integrated Backscatter (AIB):

The AIB was calculated using normalized power density spectrum from cancellous bones. The normalized power spectrum of AIB is expressed as [87]:

TABLE 5.2: *Property of the Transducer*

Parameter	Value	Parameter	Value
Central Frequency	2 MHz	R	2 cm
Number of Elements	192	d_p	0.1979 mm
w_e	0.1729 mm		

$$W(f) = \frac{\langle S_b(f) \rangle}{\langle S_{ref}(f) \rangle} \tag{5.10}$$

Where γ is the amplitude reflection coefficient, $\langle S_b(f) \rangle$ and $\langle S_{ref}(f) \rangle$ are the spatial averaged power spectrum of bone samples and the standard reflector. The $S_{ref}(f)$ for the fundamental backscatter and the 2nd harmonics are obtained seperately.

The compensation based on the probe shape is given as:

$$V_{com}(f) = (\frac{\gamma}{2})^2 \frac{3d_p^2 R^2}{2w_e^2 L A'} \tag{5.11}$$

Where d_p and w_e are the pitch and width of the transducer array elements, respectively. L stands for the range gate length, A' stands for nominal area of the transducer array and R stands for the focal length. The detailed parameters from the transducer is given in Table 5.2.

The apparent integrated backscatter is the frequency-averaged backscatter coefficient from the transducer bandwidth [55]:

$$AIB = \frac{1}{f_{max} - f_{min}} \int_{f_{min}}^{f_{max}} 8.68 ln(W(f) V_{com}(f)) df \tag{5.12}$$

The Backscatter Coefficient (BSC):

The BSC is compensated by the attenuation during the propagation in the bone sample :

$$A_{com} = (\frac{2\alpha f_0 L}{1 - e^{-2\alpha f_0 L}})^2 [1 + (\frac{2\alpha f_0 L}{2\pi})^2]^2 \tag{5.13}$$

Where α is the attenuation coefficient in the bone, R is the focal distance, L is the gated signal length.

$$BSC_{array} = V_{com} * A_{com} * \frac{1}{N} * \sum_{N}^{i=1} W(f) \tag{5.14}$$

The Spectral Centroid Shift (SCS):

In the array probe, the SCS which indicates the shift of centroid from the reference frequency $f0$ is compensated by the volume of the gated region ($V_{com}(f)$).

$$SCS_{array} = f0 - \frac{\int_{f_{min}}^{f_{max}} S_b(f) * V_{com}(f) * f * df}{\int_{f_{min}}^{f_{max}} S_b(f) * df} \tag{5.15}$$

5.5 Results and Discussion

A simplified cylinder model was used to present the correlation between trabecular thickness of cancellous bone and backscatter power spectrum. The result from Fig. 5.4 shows that the power spectrum increased with the increase of the cylinder radius.

The Pearson correlation coefficients between AIB, BSC, SCS and BMD were calculated with 95% confidence interval (Fig. 5.8). A high correlation was found in BSC of the fundamental backscatter ($R = 0.7055$, $P = 1.0551e-8$) and the second harmonics ($R = 0.7374$, $P = 1.2350e-9$). Medium to strong correlation was observed in AIB and SCS of the fundamental backscatter (AIB: $R = 0.5393$, $P = 5.3106e-5$; SCS: $R = -0.5858$, $P = 1.0083e-4$) and the second harmonics (AIB: $R = 0.6243$, $P = 3.8212e-6$; SCS: $R = -0.6421$, $P = 1.2650e-6$). In general, for both the AIB and SCS, the result from

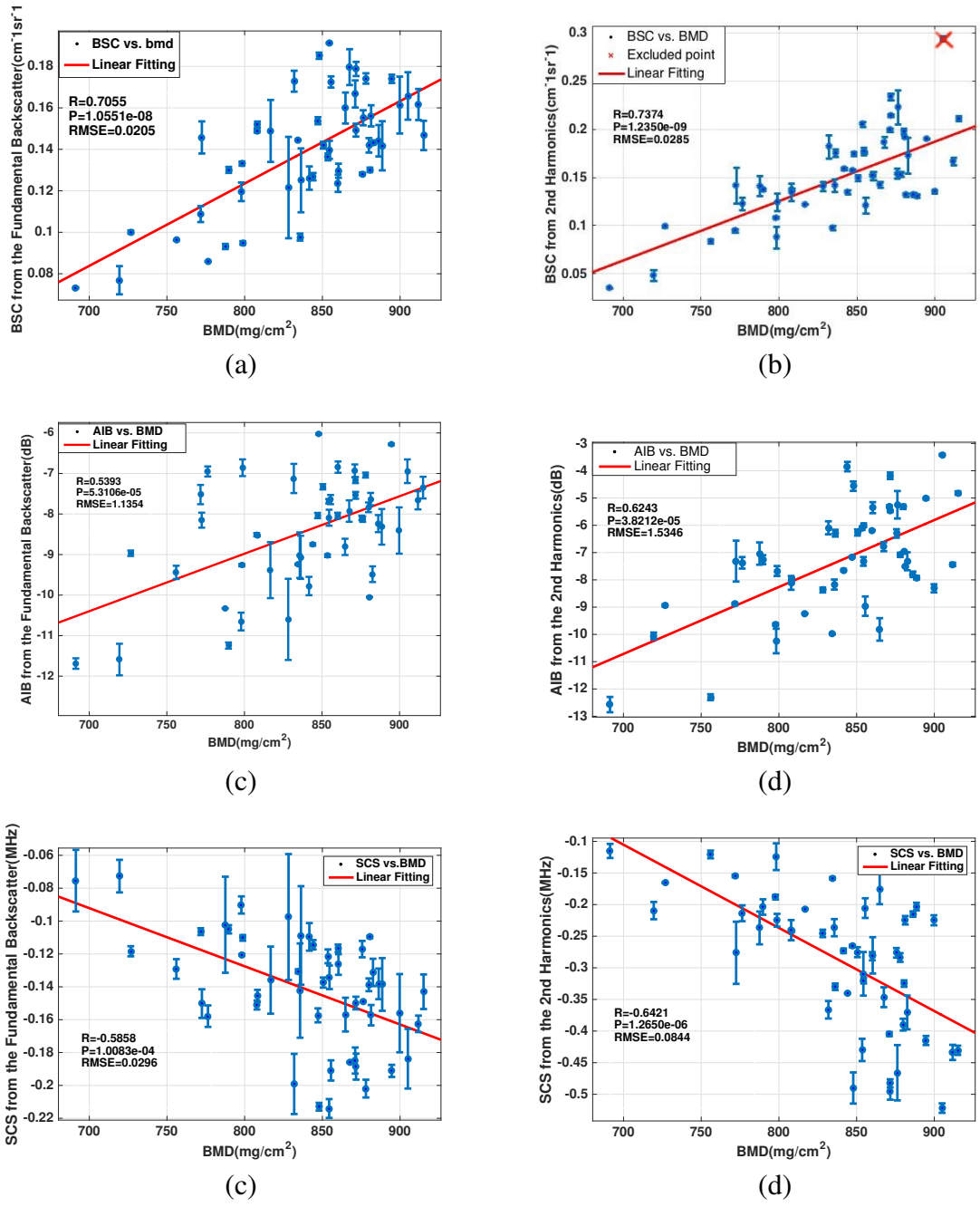

FIGURE 5.8: *The Correlation with BMD: (a) BSC from the fundamental backscatter signal. (b) BSC from the second harmonics. (c) AIB from the fundamental signal. (d) AIB from the second harmonics. (e) SCS from the fundamental signal. (f) SCS from the second harmonics.*

the second harmonics correlates better than the first harmonics. The result is consistent with the backscatter coefficient detected in soft tissue [96].

The second harmonics of the soft tissue has shown improved performance when it

comes to imaging. It improves both lateral and axial resolution, reduces side-lobes and artifacts, and reduces deleterious effects of the body wall [103]. In our study, we found that the tissue harmonic imaging technique is promising in bone mineral density measurement. This may be as the second harmonics generated contain finer information from the micro-scatters due to its high frequencies while the incident wave contains more general deep penetration information. It may also reduces multiple distortions as the second harmonic signals are along propagation of the fundamental. This is significant because in most of the existing theories and measurements, spectrum of the fundamental wave which consists of non-linearity from both the bone structure and the multiple scattering is studied, but the influence of multiple scattering is ignored for simplicity which may be one of the main reasons restraining the performance in bone density measurements. In our harmonic imaging measurement, the nonlinear effect of the bone structure is more accurately studied and thus may be a better way for bone density measurement.

Related experiments that used the similar central frequency (2MHz) to obtain BSC are from Wear et al. [37] ($f0 = 2.25MHz$, $R = 0.87$), Jenson et al. [45] ($f0 = 1MHz$, $R = 0.781$) and Padilla et al. [46] ($f0 = 1MHz$, $R = 0.61$). For AIB are from Jiang et al. [52] ($f0 = 3.5MHz$, $R = 0.55$) and Tang et al. [50] ($f0 = 3.5MHz$, $R = 0.51$), for SCS is from Garra et al. [51] ($f0 = 2.5MHz$, $R = -0.61$).Our result of AIB and SCS are of the same trend as their work. In our work we improved correlation of AIB to 0.6243, this might indicate that the apparent backscatter from the second harmonics contains finer information of the bone mineral density. However, for the BSC, we did not achieve good results as Wear's work, the reasons might be: (1) the bovine bone samples are stronger than human bones, the strong attenuation of the bone might have affected the result. The attenuation compensation function is less accurate when the signal length(L) is too long or when the attenuation (A) is too high (AL>1) [104]. (2) Our experiment and Hakulinen et al. [13] used different methods to measure the backscatter coefficient of the bone. They used the pulse-echo technique while we used the ultrasound imaging system. (3) Most of the current studies uses low frequency (<1MHz). Although those experiments achieved good result, but low frequency will lead to the lower resolution in the imaging system on

the lateral axis, which is not beneficial for signal selection and compensation.

A limitation of this study is that it used bovine bone samples rather than human bone samples. The high attenuation of bovine bones might lead to inaccuracy of correlation. The features related to imaging systems such as beamwidth, side lobes might affect the result, and this is an interesting field to explore for bone density evaluation using ultrasound imaging system in the future.

5.6 Conclusion

In this study, the apparent backscatter coefficient from the fundamental backscatter and the second harmonics were compared. The correlation from the second harmonics (R: $BSC = 0.7374$; $AIB = 0.6243$; $SCS = -0.6421$) is generally higher than from the fundamental backscatter (R: $BSC = 0.7055$; $AIB = 0.5393$; $SCS = -0.5858$). The theoretical correlation trend between the second harmonics power spectrum and the trabecular thickness was found to be positive which is the same trend as the fundamental backscatter. This might indicate that the second harmonics is able to provide BSC with improved accuracy. The improved performance may result from the less distortion and improved axial and lateral resolution of the second harmonic signal. The second harmonics is shown to be a promising indicator for bone density evaluation.

Chapter 6

Conclusion and Future Work

6.1 Conclusion

In this study, three novel research contributions that aim to evaluate the density of fetal bone were presented. The ultrasound backscatter parameters such as ultrasound backscatter coefficient (BSC), apparent integrated backscatter (AIB) and spectrum centroid shift (SCS) were used for correlation with DEXA results as well as change of bone model porosity. The key findings are listed below:

1.From the simulation study of the BSC from three probe models, the BSC from the array probe showed similar correlation with porosity but less standard deviation than the single element transducer. The BSC from the array probe was more stable than from the single element transducer and this improvement of stability might result from the wider spatial range of the array probe.

2.The COMSOL simulation result from the fetal bone model showed that with proper compensation for the tissue attenuation, the BSC was able to provide good correlation with bone porosity.Therefore, the BSC as well as AIB have potenital to become an ultrasound parameter for fetal bone density evaluation in the current commerical ultrasound imaging systems.

3.The result of BSC, AIB and SCS from the in vitro study indicates that the correlation from the bone backscatter second harmonics is higher than fundamental backscatter. And the increased result from AIB might suggest that the signal from the second harmonics contains less noise than the fundamental backscatter. The signal from the second

harmonics may be more accurate for bone density evaluation.

In conclusion, the research result in this study shows that the ultrasound backscatter coefficient correlates well with the bone mineral density. The BSC has potential to evaluate fetal bone density without ionizing radiation.

6.2 Future Work

There are several directions that are found during the research that worth exploring for:

1. **Establishing a fully automatic or semi automatic system for ultrasound backscatter estimation.** To our knowledge, most of the current backscatter estimation are evaluated manually, especially for the signal selection part. However, this part is crucial for a stable and accurate outcome, and for cases when the region of interest is out of transducer focal zone should be excluded. Based on the result from our study as well as from Conversano et al. [47], the backscatter coefficient could be evaluated from the imaging system. And it is possible to implement image processing methodologies such as imaging segmentation to select the region of interest, change of signal detection, intensity detection to exclude signals out of focal zone to evaluate backscatter coefficient efficiently.

2. **Comparing the backscatter coefficient from fetal bone data with DEXA or MRI result but rather than simulation.** In our study, a fetal simulation model was built to evaluate backscatter coefficient with the change of bone porosity. However, because there is less noise in the simulation, the simulation result is generally better than the in vivo or in vitro results. Because it is difficult to apply ethics totest on fetus or newborns, therefore the next step is to test the backscatter coefficient on the newborn animal bones, such as newborn lamb and pig femur.

3. **Backscatter correction from the interference of soft tissue.** In our study, the soft tissue thickness was measured and corrected using empirical attenuation coefficient. And there is another soft tissue correction method :using dual frequency ultrasound [66]. And this method is able to provide soft tissue thickness as well as muscle thickness. An

improved result might be obtained with the combination of the two methods to reduce the interference from the attenuation in the soft tissue.

4. **Setting a T-score standard for ultrasound backscatter evaluation.**The T-scores that are applied in DEXA are cutoffs defined by the large database with osteopenia defined as between 1 and 2.5 standard deviations and osteoporiasis more than 2.5 standard deviations below the mean density [105]. Like the T-score method in DEXA, the ultrasound backscatter result could be compared with the result in a large database of differet races, gender, age and the site of the bone. Based on the large number of the database, this standard should be more objective and more accurate for ultrasound backscatter bone density evaluation.

Bibliography

[1] P. Shipman, *The human skeleton*. Harvard University Press, 1985.

[2] R. Barkmann, P. Laugier, U. Moser, S. Dencks, M. Klausner, F. Padilla, G. Haiat, M. Heller, and C.-C. Glüer, "In vivo measurements of ultrasound transmission through the human proximal femur," *Ultrasound in medicine & biology*, vol. 34, no. 7, pp. 1186–1190, 2008.

[3] B. Brendel, S. Winter, A. Rick, M. Stockheim, and H. Ermert, "Registration of 3d ct and ultrasound datasets of the spine using bone structures," *Computer Aided Surgery*, vol. 7, no. 3, pp. 146–155, 2002.

[4] Y. Jiang, J. Zhao, E.-Y. Liao, R.-C. Dai, X.-P. Wu, and H. K. Genant, "Application of micro-ct assessment of 3-d bone microstructure in preclinical and clinical studies," *Journal of bone and mineral metabolism*, vol. 23, no. 1, pp. 122–131, 2005.

[5] V. Alt, D. V. Kögelmaier, K. S. Lips, V. Witt, S. Pacholke, C. Heiss, M. Kampschulte, S. Heinemann, T. Hanke, R. Schnettler, *et al.*, "Assessment of angiogenesis in osseointegration of a silica–collagen biomaterial using 3d-nano-ct," *Acta biomaterialia*, vol. 7, no. 10, pp. 3773–3779, 2011.

[6] K. Rathnayaka, K. I. Momot, H. Noser, A. Volp, M. A. Schuetz, T. Sahama, and B. Schmutz, "Quantification of the accuracy of mri generated 3d models of long bones compared to ct generated 3d models," *Medical engineering & physics*, vol. 34, no. 3, pp. 357–363, 2012.

[7] C. Chappard, P. Laugier, B. Fournier, C. Roux, and G. Berger, "Assessment of the relationship between broadband ultrasound attenuation and bone mineral density at the calcaneus using bua imaging and dxa," *Osteoporosis international*, vol. 7, no. 4, pp. 316–322, 1997.

[8] B. Rack, E. Lochmüller, W. Janni, G. Lipowsky, I. Engelsberger, K. Friese, and H. Küster, "Ultrasound for the assessment of bone quality in preterm and term infants," *Journal of perinatology*, vol. 32, no. 3, pp. 218–226, 2012.

[9] D. Nemet, T. Dolfin, B. Wolach, and A. Eliakim, "Quantitative ultrasound measurements of bone speed of sound in premature infants," *European journal of pediatrics*, vol. 160, no. 12, pp. 736–740, 2001.

[10] E. N. Marieb and K. Hoehn, *Human anatomy & physiology*. Pearson Education, 2007.

[11] R. Hambli and N. Hattab, "Application of neural network and finite element method for multiscale prediction of bone fatigue crack growth in cancellous bone," in *Multiscale Computer Modeling in Biomechanics and Biomedical Engineering*, pp. 3–30, Springer, 2013.

[12] R. Mueller and W. C. Hayes, "Biomechanical competence of microstructural bone in the progress of adaptive bone remodeling," in *Optical Science, Engineering and Instrumentation'97*, pp. 69–81, International Society for Optics and Photonics, 1997.

[13] M. A. Hakulinen, J. S. Day, J. Töyräs, M. Timonen, H. Kröger, H. Weinans, I. Kiviranta, and J. S. Jurvelin, "Prediction of density and mechanical properties of human trabecular bone in vitro by using ultrasound transmission and backscattering measurements at 0.2–6.7 mhz frequency range," *Physics in medicine and biology*, vol. 50, no. 8, p. 1629, 2005.

[14] S. Chaffaı, F. Peyrin, S. Nuzzo, R. Porcher, G. Berger, and P. Laugier, "Ultrasonic characterization of human cancellous bone using transmission and backscatter measurements: relationships to density and microstructure," *Bone*, vol. 30, no. 1, pp. 229–237, 2002.

[15] J. J. Watts, J. Abimanyi-Ochom, and K. M. Sanders, "Osteoporosis costing all australian: a new burden of disease analysis-2012 to 2022," 2013.

[16] P. F. Schnatz, K. A. Marakovits, and D. M. O'sullivan, "Assessment of postmenopausal women and significant risk factors for osteoporosis," *Obstetrical & gynecological survey*, vol. 65, no. 9, pp. 591–596, 2010.

[17] S. E. Painter, M. Kleerekoper, and P. M. Camacho, "Secondary osteoporosis: a review of the recent evidence," *Endocrine Practice*, 2006.

[18] B. Lecka-Czernik, "Bone loss in diabetes: use of antidiabetic thiazolidinediones and secondary osteoporosis," *Current osteoporosis reports*, vol. 8, no. 4, pp. 178–184, 2010.

[19] G. Jones, T. Nguyen, P. Sambrook, P. Kelly, and J. Eisman, "A longitudinal study of the effect of spinal degenerative disease on bone density in the elderly.," *The Journal of rheumatology*, vol. 22, no. 5, pp. 932–936, 1995.

[20] R. Hasserius, M. Karlsson, B. Nilsson, and O. Johnell, "Prevalent vertebral deformities predict increased mortality and increased fracture rate in both men and women: a 10-year population-based study of 598 individuals from the swedish cohort in the european vertebral osteoporosis study," *Osteoporosis international*, vol. 14, no. 1, pp. 61–68, 2003.

[21] K. Krishnamachari and L. Iyengar, "Effect of maternal malnutrition on the bone density of the neonates.," *The American journal of clinical nutrition*, vol. 28, no. 5, pp. 482–486, 1975.

[22] K. Godfrey, K. Walker-Bone, S. Robinson, P. Taylor, S. Shore, T. Wheeler, and C. Cooper, "Neonatal bone mass: influence of parental birthweight, maternal smoking, body composition, and activity during pregnancy," *Journal of Bone and Mineral Research*, vol. 16, no. 9, pp. 1694–1703, 2001.

[23] D. R. Carter, T. E. Orr, D. P. Fyhrie, and D. J. Schurman, "Influences of mechanical stress on prenatal and postnatal skeletal development.," *Clinical orthopaedics and related research*, vol. 219, pp. 237–250, 1987.

[24] F. Rauch and E. Schoenau, "Skeletal development in premature infants: a review of bone physiology beyond nutritional aspects," *Archives of Disease in Childhood-Fetal and Neonatal Edition*, vol. 86, no. 2, pp. F82–F85, 2002.

[25] B. MacMahon, "Prenatal x-ray exposure and childhood cancer," *Journal of the National Cancer Institute*, vol. 28, no. 5, pp. 1173–1191, 1962.

[26] D. Bulas and A. Egloff, "Benefits and risks of mri in pregnancy," in *Seminars in perinatology*, vol. 37, pp. 301–304, Elsevier, 2013.

[27] M. A. Haidekker, *Medical imaging technology*. Dordrecht: Springer, 2013.

[28] K. K. S. Nishiyama, *In Vivo Assessment of Bone Microarchitecture and Estimated Bone Strength*. PhD thesis, 2012.

[29] "Basic theory of mri." https://en.wikipedia.org/wiki/Magnetic_resonance_imaging. Accessed: 2010-09-30.

[30] B. G. Mersereau, *MRI-Guided and Compressed Sensing Reconstruction Methods for PET/MRI*. PhD thesis, 2017.

[31] E. J. Mackie, L. Tatarczuch, and M. Mirams, "The skeleton: a multi-functional complex organ. the growth plate chondrocyte and endochondral ossification," *Journal of Endocrinology*, vol. 211, no. 2, pp. 109–121, 2011.

[32] W.-Q. Cui, Y.-Y. Won, M.-H. Baek, D.-H. Lee, Y.-S. Chung, J.-H. Hur, and Y.-Z. Ma, "Age-and region-dependent changes in three-dimensional microstructural properties of proximal femoral trabeculae," *Osteoporosis International*, vol. 19, no. 11, pp. 1579–1587, 2008.

[33] S. Nuzzo, C. Meneghini, P. Braillon, R. Bouvier, S. Mobilio, and F. Peyrin, "Microarchitectural and physical changes during fetal growth in human vertebral bone," *Journal of Bone and Mineral Research*, vol. 18, no. 4, pp. 760–768, 2003.

[34] F. Jenson, F. Padilla, V. Bousson, C. Bergot, J.-D. Laredo, and P. Laugier, "In vitro ultrasonic characterization of human cancellous femoral bone using transmission and backscatter measurements:

relationships to bone mineral density," *The Journal of the Acoustical Society of America*, vol. 119, no. 1, pp. 654–663, 2006.

[35] C. Colbert, J. J. Spruit, and M. Trotter, "Estimation of gravimetric density of fetal bones from radiologic density.," *Investigative radiology*, vol. 7, no. 2, pp. 102–106, 1972.

[36] V. Roberjot, P. Laugier, P. Droin, P. Giat, and G. Berger, "Measurement of integrated backscatter coefficient of trabecular bone," in *Ultrasonics Symposium, 1996. Proceedings., 1996 IEEE*, vol. 2, pp. 1123–1126, IEEE, 1996.

[37] K. A. Wear and B. S. Garra, "Assessment of bone density using ultrasonic backscatter," *Ultrasound in medicine & biology*, vol. 24, no. 5, pp. 689–695, 1998.

[38] K. A. Wear, "Frequency dependence of ultrasonic backscatter from human trabecular bone: Theory and experiment," *The Journal of the Acoustical Society of America*, vol. 106, no. 6, pp. 3659–3664, 1999.

[39] K. A. Wear and D. W. Armstrong III, "Relationships among calcaneal backscatter, attenuation, sound speed, hip bone mineral density, and age in normal adult women," *The Journal of the Acoustical Society of America*, vol. 110, no. 1, pp. 573–578, 2001.

[40] K. A. Wear and D. Armstrong, "The relationship between ultrasonic backscatter and bone mineral density in human calcaneus.," *IEEE transactions on ultrasonics, ferroelectrics, and frequency control*, vol. 47, no. 4, pp. 777–780, 1999.

[41] K. A. Wear, A. P. Stuber, and J. C. Reynolds, "Relationships of ultrasonic backscatter with ultrasonic attenuation, sound speed and bone mineral density in human calcaneus," *Ultrasound in medicine & biology*, vol. 26, no. 8, pp. 1311–1316, 2000.

[42] K. A. Wear and A. Laib, "The dependence of ultrasonic backscatter on trabecular thickness in human calcaneus: theoretical and experimental results," *Ultrasonics, Ferroelectrics, and Frequency Control, IEEE Transactions on*, vol. 50, no. 8, pp. 979–986, 2003.

[43] S. Chaffaı, V. Roberjot, F. Peyrin, G. Berger, and P. Laugier, "Frequency dependence of ultrasonic backscattering in cancellous bone: Autocorrelation model and experimental results," *The Journal of the Acoustical Society of America*, vol. 108, no. 5, pp. 2403–2411, 2000.

[44] C. Roux, V. Roberjot, R. Porcher, S. Kolta, M. Dougados, and P. Laugier, "Ultrasonic backscatter and transmission parameters at the os calcis in postmenopausal osteoporosis," *Journal of Bone and Mineral Research*, vol. 16, no. 7, pp. 1353–1362, 2001.

[45] F. Jenson, F. Padilla, F. Peyrin, P. Cloetens, V. Bousson, C. Bergot, J.-D. Laredo, C. Latremouille, and P. Laugier, "Characterization of human femoral trabecular bone in vitro using transmission and

backscatter ultrasound measurements," in *Ultrasonics Symposium, 2004 IEEE*, vol. 1, pp. 569–572, IEEE, 2004.

[46] F. Padilla, F. Jenson, V. Bousson, F. Peyrin, and P. Laugier, "Relationships of trabecular bone structure with quantitative ultrasound parameters: in vitro study on human proximal femur using transmission and backscatter measurements," *Bone*, vol. 42, no. 6, pp. 1193–1202, 2008.

[47] F. Conversano, R. Franchini, A. Greco, G. Soloperto, F. Chiriacò, E. Casciaro, M. Aventaggiato, M. D. Renna, P. Pisani, M. Di Paola, *et al.*, "A novel ultrasound methodology for estimating spine mineral density," *Ultrasound in medicine & biology*, vol. 41, no. 1, pp. 281–300, 2015.

[48] R. Zhang, D. Ta, C. Liu, and C. Chen, "Feasibility of bone assessment with ultrasonic backscatter signals in neonates," *Ultrasound in medicine & biology*, vol. 39, no. 10, pp. 1751–1759, 2013.

[49] K. A. Wear, "Characterization of trabecular bone using the backscattered spectral centroid shift," *Ultrasonics, Ferroelectrics, and Frequency Control, IEEE Transactions on*, vol. 50, no. 4, pp. 402–407, 2003.

[50] T. Tang, C. Liu, F. Xu, and D. Ta, "Correlation between the combination of apparent integrated backscatter–spectral centroid shift and bone mineral density," *Journal of Medical Ultrasonics*, pp. 1–7, 2016.

[51] B. S. Garra, M. Locher, S. Felker, and K. A. Wear, "Measurements of ultrasonic backscattered spectral centroid shift from spine in vivo: methodology and preliminary results," *Ultrasound in medicine & biology*, vol. 35, no. 1, pp. 165–168, 2009.

[52] Y.-q. Jiang, C.-c. Liu, R.-y. Li, W.-P. Wang, H. Ding, Q. Qi, D. Ta, J. Dong, and W.-q. Wang, "Analysis of apparent integrated backscatter coefficient and backscattered spectral centroid shift in calcaneus in vivo for the ultrasonic evaluation of osteoporosis," *Ultrasound in medicine & biology*, vol. 40, no. 6, pp. 1307–1317, 2014.

[53] B. Hoffmeister, C. Jones III, G. Caldwell, and S. Kaste, "Ultrasonic characterization of cancellous bone using apparent integrated backscatter," *Physics in medicine and biology*, vol. 51, no. 11, p. 2715, 2006.

[54] B. K. Hoffmeister, D. P. Johnson, J. A. Janeski, D. A. Keedy, B. W. Steinert, A. M. Viano, and S. C. Kaste, "Ultrasonic characterization of human cancellous bone in vitro using three different apparent backscatter parameters in the frequency range 0.6-15.0 mhz," *Ultrasonics, Ferroelectrics, and Frequency Control, IEEE Transactions on*, vol. 55, no. 7, pp. 1442–1452, 2008.

[55] M. Malo, J. Töyräs, J. Karjalainen, H. Isaksson, O. Riekkinen, and J. Jurvelin, "Ultrasound backscatter measurements of intact human proximal femurs—relationships of ultrasound parameters with tissue structure and mineral density," *Bone*, vol. 64, pp. 240–245, 2014.

[56] F. rédéric Jenson, F. rédéric Padilla, and P. Laugier, "Prediction of frequency-dependent ultrasonic backscatter in cancellous bone using statistical weak scattering model," *Ultrasound in medicine & biology*, vol. 29, no. 3, pp. 455–464, 2003.

[57] K. I. Lee, "Dependences of the attenuation and the backscatter coefficients on the frequency and the porosity in bovine trabecular bone: Application of the binary mixture model," *Journal of the Korean Physical Society*, vol. 60, no. 3, pp. 371–375, 2012.

[58] D. Ta, W. Wang, K. Huang, Y. Wang, and L. H. Le, "Analysis of frequency dependence of ultrasonic backscatter coefficient in cancellous bone," *The Journal of the Acoustical Society of America*, vol. 124, no. 6, pp. 4083–4090, 2008.

[59] K. A. Wear and G. R. Harris, "Frequency dependence of backscatter from thin, oblique, finite-length cylinders measured with a focused transducer-with applications in cancellous bone," *The Journal of the Acoustical Society of America*, vol. 124, no. 5, pp. 3309–3314, 2008.

[60] K. I. Lee, "Dependences of the backscatter coefficient on the frequency, the bone volume fraction, and the trabecular thickness in bovine femoral trabecular bone in vitro," *Journal of the Korean Physical Society*, vol. 63, no. 5, pp. 991–995, 2013.

[61] U. Sockalin and C. Zhang, "Experimental analysis of binary mixture model for ultrasound scattering from cancellous bone," in *Industrial Electronics and Applications (ICIEA), 2010 the 5th IEEE Conference on*, pp. 1681–1685, IEEE, 2010.

[62] B. K. Hoffmeister, "Frequency dependence of apparent ultrasonic backscatter from human cancellous bone," *Physics in medicine and biology*, vol. 56, no. 3, p. 667, 2011.

[63] B. Yang, D. Ta, K. Huang, and W. Wang, "Characterization of cancellous bone microstructure by using ultrasonic apparent backscatter imaging," in *Biomedical Engineering and Informatics, 2009. BMEI'09. 2nd International Conference on*, pp. 1–5, IEEE, 2009.

[64] D. Ta, K. Huang, and W. Wang, "Correlations between signal spectrum of ultrasonic backscatter and cancellous bone microstructure," in *Ultrasonics Symposium (IUS), 2009 IEEE International*, pp. 1–4, IEEE, 2009.

[65] J. P. Karjalainen, J. Töyräs, O. Riekkinen, M. Hakulinen, and J. S. Jurvelin, "Ultrasound backscatter imaging provides frequency-dependent information on structure, composition and mechanical properties of human trabecular bone," *Ultrasound in medicine & biology*, vol. 35, no. 8, pp. 1376–1384, 2009.

[66] O. Riekkinen, M. Hakulinen, J. Töyräs, and J. Jurvelin, "Dual-frequency ultrasound—new pulse–echo technique for bone densitometry," *Ultrasound in medicine & biology*, vol. 34, no. 10, pp. 1703–1708, 2008.

[67] B. K. Hoffmeister, A. R. Wilson, M. J. Gilbert, and M. E. Sellers, "A backscatter difference technique for ultrasonic bone assessment," *The Journal of the Acoustical Society of America*, vol. 132, no. 6, pp. 4069–4076, 2012.

[68] B. A. Angelsen, "Ultrasound imaging," *Waves, Signals and Signal Processing. Emantec, Trondheim, Norway*, 2000.

[69] P. Zioupos, R. B. Cook, and J. R. Hutchinson, "Some basic relationships between density values in cancellous and cortical bone," *Journal of biomechanics*, vol. 41, no. 9, pp. 1961–1968, 2008.

[70] F. P. Hadlock, R. Harrist, R. S. Sharman, R. L. Deter, and S. K. Park, "Estimation of fetal weight with the use of head, body, and femur measurements—a prospective study," *American journal of obstetrics and gynecology*, vol. 151, no. 3, pp. 333–337, 1985.

[71] C. Cooper, M. Javaid, P. Taylor, K. Walker-Bone, E. Dennison, and N. Arden, "The fetal origins of osteoporotic fracture," *Calcified tissue international*, vol. 70, no. 5, pp. 391–394, 2002.

[72] X. Yan, M.-J. Zhu, M. V. Dodson, and M. Du, "Developmental programming of fetal skeletal muscle and adipose tissue development," *Journal of genomics*, vol. 1, pp. 29–38, 2013.

[73] H. McDevitt and S. Ahmed, "Quantitative ultrasound assessment of bone health in the neonate," *Neonatology*, vol. 91, no. 1, pp. 2–11, 2006.

[74] V. Gilsanz, "Bone density in children: a review of the available techniques and indications," *European journal of radiology*, vol. 26, no. 2, pp. 177–182, 1998.

[75] Y. J. Yoon, J.-P. Chung, C.-S. Bae, and S.-Y. Han, "The speed of sound through trabecular bone predicted by biot theory," *Journal of biomechanics*, vol. 45, no. 4, pp. 716–718, 2012.

[76] K. I. Lee and S. W. Yoon, "Comparison of acoustic characteristics predicted by biot's theory and the modified biot–attenborough model in cancellous bone," *Journal of biomechanics*, vol. 39, no. 2, pp. 364–368, 2006.

[77] R. Strelitzki, P. Nicholson, and V. Paech, "A model for ultrasonic scattering in cancellous bone based on velocity fluctuations in a binary mixture," *Physiological measurement*, vol. 19, no. 2, p. 189, 1998.

[78] M. Fellah, Z. E. A. Fellah, F. Mitri, E. Ogam, and C. Depollier, "Transient ultrasound propagation in porous media using biot theory and fractional calculus: Application to human cancellous bone," *The Journal of the Acoustical Society of America*, vol. 133, no. 4, pp. 1867–1881, 2013.

[79] M. Sadouki, M. Fellah, Z. Fellah, E. Ogam, and C. Depollier, "Ultrasonic propagation of reflected waves in cancellous bone: Application of biot theory," in *Ultrasonic Characterization of Bone (ES-UCB), 2015 6th European Symposium on*, pp. 1–4, IEEE, 2015.

[80] J. L. Buchanan, R. P. Gilbert, and M.-j. Ou, "Transfer functions for a one-dimensional fluid–poroelastic system subject to an ultrasonic pulse," *Nonlinear Analysis: Real World Applications*, vol. 13, no. 3, pp. 1030–1043, 2012.

[81] V.-H. Nguyen, S. Naili, and V. Sansalone, "Simulation of ultrasonic wave propagation in anisotropic cancellous bone immersed in fluid," *Wave Motion*, vol. 47, no. 2, pp. 117–129, 2010.

[82] H. J. Camin and M. J. Isakson, "A comparison of sediment reflection coefficient measurements to elastic and poro-elastic models," *The Journal of the Acoustical Society of America*, vol. 120, no. 5, pp. 2437–2449, 2006.

[83] R. D. Stoll and T.-K. Kan, "Reflection of acoustic waves at a water–sediment interface," *The Journal of the Acoustical Society of America*, vol. 70, no. 1, pp. 149–156, 1981.

[84] T. Haire and C. Langton, "Biot theory: a review of its application to ultrasound propagation through cancellous bone," *Bone*, vol. 24, no. 4, pp. 291–295, 1999.

[85] M. A. Biot, "Theory of propagation of elastic waves in a fluid-saturated porous solid. i. low-frequency range," *The Journal of the acoustical Society of america*, vol. 28, no. 2, pp. 168–178, 1956.

[86] M. A. Biot, "Theory of propagation of elastic waves in a fluid-saturated porous solid. ii. higher frequency range," *the Journal of the Acoustical Society of America*, vol. 28, no. 2, pp. 179–191, 1956.

[87] M. Insana, T. Hall, and L. Cook, "Backscatter coefficient estimation using array transducers," *IEEE transactions on ultrasonics, ferroelectrics, and frequency control*, vol. 41, no. 5, pp. 714–723, 1994.

[88] T. Oguri, K. Tamura, K. Yoshida, J. Mamou, H. Hasegawa, H. Maruyama, H. Hachiya, and T. Yamaguchi, "Estimation of scatterer size and acoustic concentration in sound field produced by linear phased array transducer," *Japanese Journal of Applied Physics*, vol. 54, no. 7S1, p. 07HF14, 2015.

[89] P. Laugier and G. Haïat, *Bone quantitative ultrasound*, vol. 576. Springer, 2011.

[90] I. R. Kamel, "An evaluation of overlying tissues to determine fetal exposure to ultrasound during the third trimester," *Ultrasound in medicine & biology*, vol. 20, no. 1, pp. 41–51, 1994.

[91] M. Scioscia, F. Scioscia, A. Vimercati, F. Caradonna, C. Nardelli, L. R. Pinto, and L. E. Selvaggi, "Estimation of fetal weight by measurement of fetal thigh soft-tissue thickness in the late third trimester," *Ultrasound in Obstetrics & Gynecology*, vol. 31, no. 3, pp. 314–320, 2008.

[92] F. P. Hadlock, R. Harrist, R. L. Deter, and S. K. Park, "Fetal femur length as a predictor of menstrual age: sonographically measured," *American Journal of Roentgenology*, vol. 138, no. 5, pp. 875–878, 1982.

[93] X. Su, Q. Feng, F. Cui, and X. Zhu, "Microstructure and micromechanical properties of the mid-diaphyses of human fetal femurs," *Connective tissue research*, vol. 36, no. 3, pp. 271–286, 1997.

[94] K. A. Wear, "Ultrasonic scattering from cancellous bone: a review," *Ultrasonics, Ferroelectrics, and Frequency Control, IEEE Transactions on*, vol. 55, no. 7, pp. 1432–1441, 2008.

[95] M. A. Averkiou, D. N. Roundhill, and J. Powers, "A new imaging technique based on the nonlinear properties of tissues," in *Ultrasonics Symposium, 1997. Proceedings., 1997 IEEE*, vol. 2, pp. 1561–1566, IEEE, 1997.

[96] T. A. Beaver, A. Jansujwicz, B. E. Arbuckle, A. D'Sa, and R. T. Palac, "Integrated backscatter during harmonic and fundamental frequency imaging—effect of depth, mechanical index, and tissue anisotropy: Implications for myocardial tissue characterization," *Echocardiography*, vol. 20, no. 4, pp. 337–343, 2003.

[97] Y. Jing, *Physics of tissue harmonic imaging by ultrasound*. 2005.

[98] D. H. Simpson, C. T. Chin, and P. N. Burns, "Pulse inversion doppler: a new method for detecting nonlinear echoes from microbubble contrast agents," *IEEE transactions on ultrasonics, ferroelectrics, and frequency control*, vol. 46, no. 2, pp. 372–382, 1999.

[99] B. K. Hoffmeister, M. R. Smathers, C. J. Miller, J. A. McPherson, C. R. Thurston, P. L. Spinolo, and S.-R. Lee, "Backscatter difference measurements of cancellous bone using an ultrasonic imaging system," *Ultrasonic imaging*, p. 0161734615603703, 2015.

[100] I. Abbasov, "Study of the second harmonics in nonlinear scattering of interacting acoustic waves by a rigid cylinder," *Acoustical Physics*, vol. 47, no. 6, pp. 633–639, 2001.

[101] J. J. Faran Jr, "Sound scattering by solid cylinders and spheres," *The Journal of the acoustical society of America*, vol. 23, no. 4, pp. 405–418, 1951.

[102] G. Renaud, S. Callé, J.-P. Remenieras, and M. Defontaine, "Non-linear acoustic measurements to assess crack density in trabecular bone," *International Journal of Non-Linear Mechanics*, vol. 43, no. 3, pp. 194–200, 2008.

[103] S. Choudhry, B. Gorman, J. W. Charboneau, D. J. Tradup, R. J. Beck, J. M. Kofler, and D. S. Groth, "Comparison of tissue harmonic imaging with conventional us in abdominal disease 1," *Radiographics*, vol. 20, no. 4, pp. 1127–1135, 2000.

[104] M. L. Oelze and W. D. O'Brien Jr, "Frequency-dependent attenuation-compensation functions for ultrasonic signals backscattered from random media," *The Journal of the Acoustical Society of America*, vol. 111, no. 5, pp. 2308–2319, 2002.

[105] B. Forogh, A. Ghasemzadeh, and A. Salimzadeh, "Comparison of bone mineral density measured by dual x-ray, axial dual-energy photon x-ray absorptiometry and laser absorptiometry of calcaneus," *Iranian Journal of Medical Sciences*, vol. 30, no. 1, pp. 34–37, 2015.